Adaptive Control of Hypersonic Vehicles in Presence of Actuation Uncertainties

by

Amith Somanath

Submitted to the Department of Aeronautics and Astronautics
in partial fulfillment of the requirements for the degree of

Master of Science in Aeronautics and Astronautics

at the

MASSACHUSETTS INSTITUTE OF TECHNOLOGY

June 2010

ARCHIVES
MASSACHUSETTS INSTITUTE
OF TECHNOLOGY
JUN 2 3 2010
LIBRARIES

© Massachusetts Institute of Technology 2010. All rights reserved.

Author ....
Department of Aeronautics and Astronautics
May 15, 2010

Certified by..
Dr Anuradha Annaswamy
Senior Research Scientist, Dept of Mechanical Engineering
Thesis Supervisor

Accepted by..
Prof Eytan H. Modiano
Associate Professor of Aeronautics and Astronautics
Chair, Committee on Graduate Students

Adaptive Control of Hypersonic Vehicles in Presence of Actuation Uncertainties

by

Amith Somanath

Submitted to the Department of Aeronautics and Astronautics
on May 15, 2010, in partial fulfillment of the
requirements for the degree of
Master of Science in Aeronautics and Astronautics

Abstract

The thesis develops a new class of adaptive controllers that guarantee global stability in presence of actuation uncertainties. Actuation uncertainties culminate to linear plants with a partially known input matrix B. Currently available multivariable adaptive controllers yield global stability only when the input matrix B is completely known. It is shown in this work that when additional information regarding the structure of B is available, this difficulty can be overcome using the proposed class of controllers. In addition, a nonlinear damping term is added to the adaptive law to further improve the stability characteristics.

It is shown here that the adaptive controllers developed above are well suited for command tracking in hypersonic vehicles (HSV) in the presence of aerodynamic and center of gravity (CG) uncertainties. A model that accurately captures the effect of CG shifts on the longitudinal dynamics of the HSV is derived from first principles. Linearization of these nonlinear equations about an operating point indicate that a constant gain controller does not guarantee vehicle stability, thereby motivating the use of an adaptive controller. Performance improvements are shown using simulation studies carried out on a full scale nonlinear model of the HSV. It is shown that the tolerable CG shifts can be almost doubled by using an adaptive controller as compared to a linear controller while tracking reference commands in velocity and altitude.

Thesis Supervisor: Dr Anuradha Annaswamy
Title: Senior Research Scientist, Dept of Mechanical Engineering

Acknowledgments

I would like to thank Dr. Anuradha Annaswamy for her invaluable guidance, motivation and support throughout the course of my master's program.

I would also like to thank my lab mates Travis Gibson, Megumi Matsutani, Manohar Srikanth and Zac Dydek for making my stay at the lab enjoyable.

I would like to express my sincere gratitude to my parents for their continuous support and encouragement without which this work would have not been possible. This thesis is dedicated to them.

This work is supported by NASA award NNX07AC48A

Contents

1 Introduction **13**

1.1 Hypersonic Vehicles 13

1.2 Actuation Uncertainties and Adaptive Control 17

1.3 Plant Uncertainties in Hypersonic Vehicles 18

1.4 Outline 19

2 Adaptive Control in presence of actuation uncertainties **21**

2.1 Problem Statement 22

2.1.1 Known B 22

2.1.2 Unknown B 24

2.2 Adaptive controller for systems with partially known input matrix B 26

2.2.1 $B = \Lambda B_p$: Uncertainties in plant dynamics 28

2.2.2 $B = B_p \Lambda$: Anomalies in actuators 29

2.3 Adaptive Control with nonlinear damping 30

2.3.1 Illustrative scalar example 31

2.3.2 Stability proof 32

3 Modeling the HSV **35**

3.1 Rigid Body Model 37

3.2 Propulsion Model 39

3.3 Elastic Model 42

3.4 Equations of Motion 44

4 Nonlinear model for Center of Gravity Uncertainty 47
4.1 Nonlinear model for Center of Gravity shifts 49
4.2 Linearization 53
4.2.1 Linearized Model of the HSV 53
4.2.2 Effect of CG shift on dynamics 54

5 Application to Hypersonic Vehicles 57
5.1 Control Architecture 59
5.2 Linear Controller Design 61
5.3 Adaptive Controller Design 63
5.4 Simulation Studies 64

6 Conclusion 67

A Hypersonic Vehicle Data 69

List of Figures

1-1 Artistic impression of the HSV 13
1-2 Artistic impression hypersonic transport 14
1-3 3-view of X-43 A 15
1-4 Typical mission profile of X-43 16

2-1 Adaptive control with Nonlinear Damping I 31
2-2 Adaptive control with Nonlinear Damping II 32

3-1 HSV side view I 35
3-2 HSV side view II 37
3-3 Oblique Shock/ Prandtl Meyer Theory 38
3-4 Schematic of Scramjet Engine 39
3-5 Assumed Modes Method 42

4-1 Axes of HSV 50

5-1 Eigenvalues of the HSV 57
5-2 Altitude and Phugoid modes 58
5-3 Adaptive Control Architecture 60
5-4 Trim trajectory 61
5-5 Controller Tracking 65
5-6 Controller performance : Rigid States 65
5-7 Controller performance : Flexible States 66
5-8 Controller performance : Control Inputs 66

List of Tables

4.1 Variation of trim points as a function of CG movement 54

5.1 Trim values for HSV 59

A.1 Geometric and Atmospheric Data 69
A.2 Lift, Drag, Thrust and Moment co-efficients 70
A.3 Elastic co-efficients 71

Chapter 1

Introduction

1.1 Hypersonic Vehicles

The *Hypersonic Vehicle* (HSV) program is mainly being pursued as it promises to provide a reliable and cost effective access to space. The hypersonic vehicles are air-breathing as compared to their rocket fuel based counterparts, thereby signifi-

Figure 1-1: Artistic impression of the HSV [1]

cantly reducing operating costs and increasing payload carrying capabilities. Air-breathing vehicles not only increase propulsion efficiency but also make the vehicle highly reusable, further reducing cost [2, 3]. The concept of using hypersonic vehicles for commercialized transport is a topic of active research (Figure 1-2). As hypersonic vehicles operate at speeds of Mach 5-7, it is estimated that if such a technology becomes viable, flight time from New York to Tokyo can be reduced to merely 2 hours!

The goals of the HSV program are two-fold : (i) to generate a first principle dynamical model of the vehicle and (ii) to design a controller for the cruise phase. Modeling and control design of such vehicles has been a challenge as the dynamics involve strong coupling of aerodynamic, structural and propulsion effects. The long and slender geometry of the HSV is primarily designed to generate a weak shock at the inlet of the scramjet engine in order to increase the propulsion efficiency. However, the vehicle can no longer be assumed rigid and flexible effects must be explicitly taken into account in the vehicle dynamics. To ensure that the hypersonic vehicle operates at a high aerodynamic efficiency for a large range of operating conditions, aircraft designers are forced to design such vehicles open loop unstable. This leads to an additional challenge that the HSV would not be operable without a flight stability augmentation system or what is commonly referred to as an autopilot.

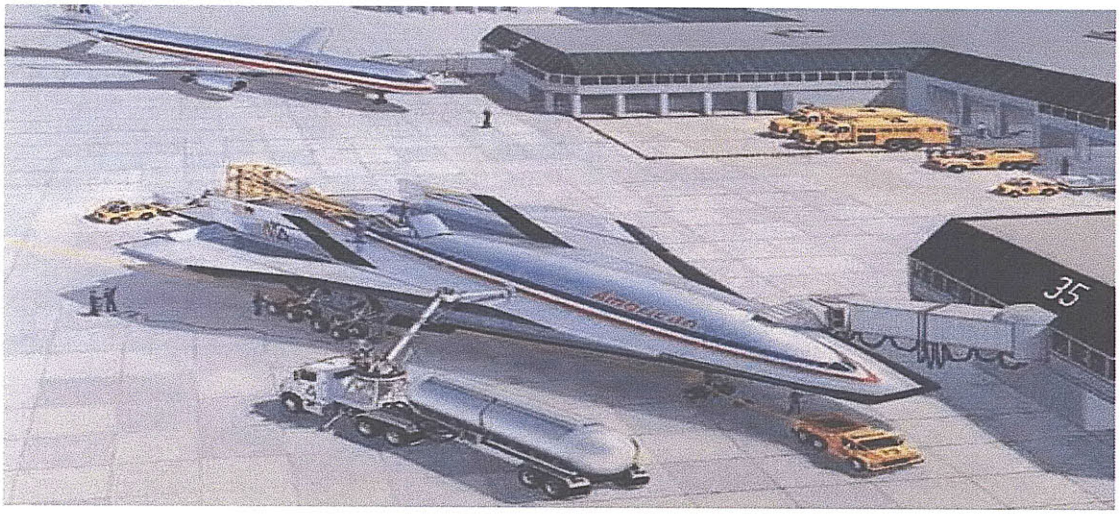

Figure 1-2: Artistic impression of hypersonic transport [1]

Active research in hypersonic vehicles began in 1996, with the development of first scramjet engine powered hypersonic vehicle, the X-43A by NASA (Figures 1-1 and 1-3). The concept demonstrator experimental vehicle was 12 ft long, 5 ft wide and weighed about 3000 pounds. This scaled down version of the hypersonic vehicle was mainly intended to flight-validate scramjet propulsion, high speed aerodynamics and design methods. There have been three experimental flights till date, the first one of which was a failure, where as the other two have flown successfully; with the scramjet operating for 10 seconds, followed by a 10 min glide and intentional crash into the pacific ocean [3].

The most notable flight of the X-43A took place on November 16, 2004, when the vehicle clocked a flight speed of Mach 9.8, successfully demonstrating the hypersonic concept. Figure 1-4 describes a typical mission profile of the X-43A in detail. As the scramjet engine cannot self start at low speeds, the HSV needs to be air launched. The hypersonic vehicle (X-43A) starts its journey at the nose of a Pegasus booster which is under-wing a B-52 aircraft. The B-52 carries the booster and the hypersonic vehicle to an altitude of 45 000 ft. At this stage, the booster detaches from the mother

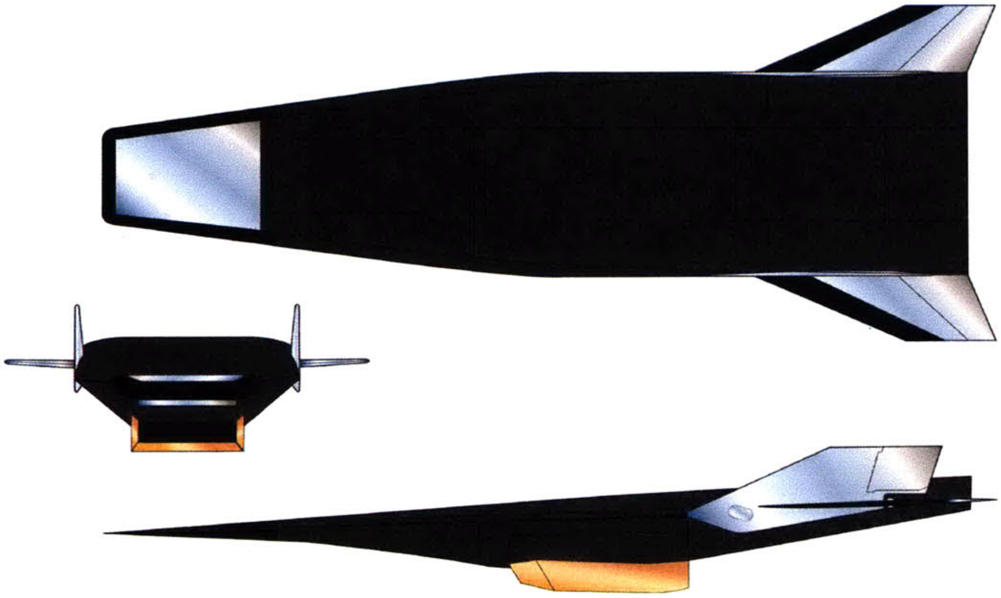

Figure 1-3: 3-view of X-43 A [1]

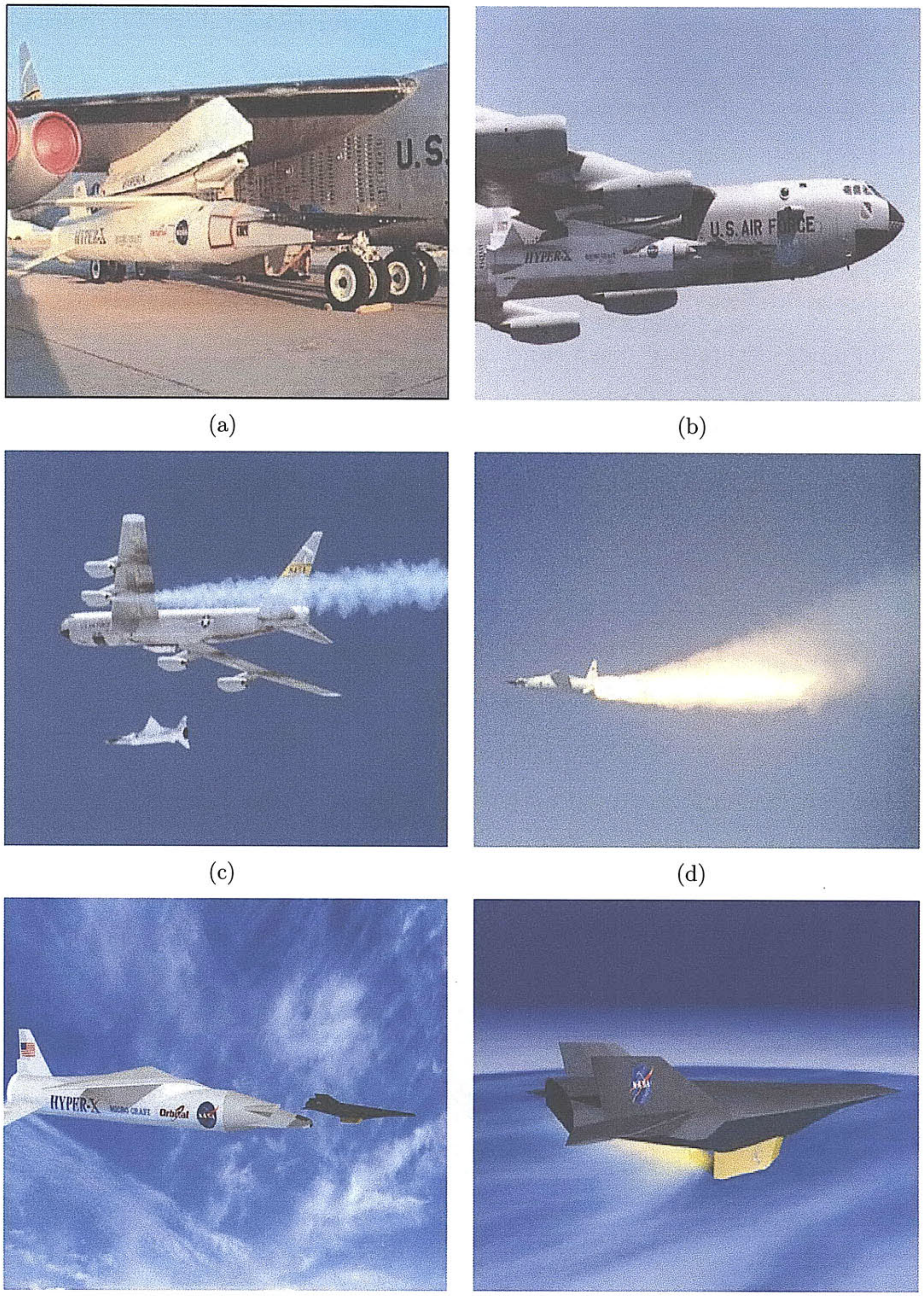
(a) (b) (c) (d) (e) (f)

U.S.
HYPER-X
U.S. AIR FORCE
HYPER-X
HYPER-X
Orbital

Figure 1-4: Typical Mission profile of X-43 [1] (a) X-43 (black) attached to Pegasus booster (white) underwing B-52 (b) B-52 takes off with the booster (c) Pegasus Booster separates from B-52 (d) Booster fires HSV to its cruise altitude (e) HSV detaches from booster (f) HSV in cruise phase

aircraft and carries X-43A to its cruise altitude of 95 000 ft. When the booster burns out, the scramjet engine is initiated and the X-43 separates from the booster cruising at a speed of Mach 8.

1.2 Actuation Uncertainties and Adaptive Control

Consider the linear dynamical system,

$$\dot{x} = Ax + Bu \tag{1.1}$$

Actuation uncertainties can be defined as all those uncertainties that lead to changes in the control matrix B. Actuation uncertainties arise due to anomalies that occur either in the plant dynamics or in actuators. Variations in plant parameters can change the way the control inputs effect the plant dynamics. Actuator failures can lead to loss of actuator effectiveness. Under such conditions, precise information about the control matrix B is not available. Control laws that do not explicitly account for actuation uncertainties can result in poor system performance and in some cases, lead to system instability.

The strength of multivariable adaptive control lies in the fact that global stability of (1.1) can be guaranteed for any unknown A as long as control matrix B is fully known and the pair (A, B) remains controllable. The time varying gain "adapts" to the changes in A based on the error between the current value of state $x(t)$ and the desired value of state $x_m(t)$. Intuitively, this is the essence of Model Reference Adaptive Control (MRAC) (see [4] for details).

However, it is well known that currently available adaptive control techniques only yield local stability results for a general unknown B. This work tries to bridge this gap in the literature by deriving a globally stable adaptive controller when additional information regarding the structure of matrix B is known. As it would be shown, the assumptions made regarding the structure of B, are in fact quite general and can be used to address a large class of problems that arise due to actuation uncertainties.

1.3 Plant Uncertainties in Hypersonic Vehicles

Apart from being open loop unstable and geometrically flexible, the HSV is also subjected to various uncertainties. Due to harsh, uncertain and varying operating conditions and limited wind-tunnel data, aerodynamic parameters such as lift and moment co-efficients of the vehicle are not well known. Mass flow spillage and changes in the diffuser area ratio can result in variations in the thrust produced by the scramjet engine. The vehicle actuators, namely the elevator and the canard are subject to various anomalies including loss of effectiveness, actuator lock and saturation. As the uncertainties cannot be predicted before hand, an adaptive controller that can cope with many of these uncertainties is highly desirable [5, 6, 7, 8].

Various uncertainties have been addressed in the context of the HSV, which include geometric and inertial [7, 9, 10], aerodynamic [5, 6], inertial elastic [8] and thrust uncertainties [11]. In this work, we consider an additional class of uncertainties which occur due to center of gravity (CG) movements. CG movements directly impact the irregular short-period mode of the HSV. Even small shifts in CG can introduce further instabilities, causing large changes in the dynamics of the HSV, as well as excite the flexible dynamics. Since the conservation equations of the HSV are derived by evaluating forces and moments about the CG, even the linearized equations of motion get altered when the CG moves.

A comprehensive study of the CG movement has been carried out in [12] where a set of generalized equations of motion for a rigid aircraft is derived from first principles, referenced about an arbitrary fixed point on the body. Using this model, in this work we derive the effects of the CG shift on the longitudinal dynamics of the aircraft. We further show that using a correct stability axis transformation, the effect of the CG movement on the dynamics can be accurately modeled, which occurs in a transparent manner in the corresponding linearized model.

The starting point for the controller proposed in this work is the representation of the aerodynamic and center of gravity uncertainties mentioned above as a class of parametric uncertainties in the underlying linear plant-model. As it would be shown, despite the accessibility of all states of this model for control, existing results in multivariable adaptive control are inapplicable. As a result, a new controller is derived and is shown to globally stabilize the linear plant for this class of parametric uncertainties. The adaptive controller proposed is validated using simulation studies on a high fidelity nonlinear model of the HSV identified from literature. The results show the advantage of adaptation compared to a baseline, non-adaptive controller, for a range of CG movements.

1.4 Outline

Chapter 2 : A new class of adaptive controllers that guarantee global stability in presence of actuation uncertainties are developed in this chapter. When a plant is subjected to actuation uncertainties, only partial information is available about the control matrix B. Global stability results are available when B is completely known, but existing multivariable adaptive controllers yield only local stability results for a general unknown B. The study fills the gap in literature by deriving a controller that is globally stable if the control matrix B is unknown, but satisfies a broad set of assumptions.

Chapter 3 : This chapter discusses the current state of art in vehicle modeling and describes in detail various vehicles models of the HSV available in the literature. Out of these, a high fidelity model has been identified to validate the control designs developed in this work.

Chapter 4 : A nonlinear model for Center of Gravity (CG) uncertainty is derived from first principles. This model is then linearized and insights are developed for control design. It is shown that a linear controller is in general, unable to guarantee stability for HSV under CG movements, thus calling for an adaptive controller.

Chapter 5 : The control design developed in Chapter 2 is validated on the HSV in presence of CG movements (developed in Chapter 3 and 4). The HSV satisfies the general assumptions required by the proposed adaptive controllers, thereby making them applicable for a large range of CG movements. Simulation studies performed on the HSV show that the adaptive controller yields superior performance over linear control designs for a large range of CG movements, while tracking reference commands in velocity and altitude.

Chapter 6 : The main contributions of this work are enlisted in this chapter.

Chapter 2

Adaptive Control in presence of actuation uncertainties

The new adaptive controllers proposed in this chapter consist of two novel extensions to the standard multivariable adaptive controllers that are well known in the literature [4]. The first is the consideration of uncertainties in the input-matrix B. It is well known that when B is completely known or when B includes only scaled-uncertainties [13, 14] , a globally stabilizing adaptive controller can be constructed, and that for a general unknown B, only local stability results are available [4]. In this chapter, the former class is expanded further if the class of uncertainties in B satisfy a broad set of assumptions. These assumptions are in fact quite general and can be used to address a large class of problems.

The second innovation introduced in the proposed adaptive controller is the use of nonlinear damping. Employed in the past for addressing difficulties introduced due to relative degree [4], the introduction of nonlinear damping here is shown to result in a stable controller and in a better performance in the simulation studies. These two extensions are the main contributions of this thesis.

2.1 Problem Statement

Consider the MIMO plant with dynamics,

$$\dot{x} = Ax + Bu \tag{2.1}$$

where the state $x \in \Re^{n\times 1}$ is accessible and $u \in \Re^{m\times 1}$ is the control input. The problem is to determine u when A and B are unknown so that the closed-loop system is stabilized and the state x is brought to zero. This problem has been studied extensively [4] and several global and local results are available. Since these results are pertinent to the contribution of this thesis, we briefly review the relevant results in this area.

2.1.1 Known B

The simplest adaptive controller that can be derived when states are accessible corresponds to the case when A is unknown in (2.1) but B is completely known. Under the assumption that there exists a θ^* such that,

$$A + B\theta^* = A_m \tag{2.2}$$

where A_m is a known Hurwitz matrix, it can easily be shown that the following adaptive controller leads to global stability.

$$u = \theta x \tag{2.3}$$

$$\dot{\theta} = -\Gamma B^T P e x^T \tag{2.4}$$

$$e = x - x_m, \quad \dot{x}_m = A_m x_m \tag{2.5}$$

where P satisfies the Lyapunov equation

$$A_m^T P + P A_m = -Q < 0. \tag{2.6}$$

The corresponding Lyapunov function in this case is of the form

$$V = e^T Pe + Trace(\tilde{\theta}^T\ \Gamma^{-1}\ \tilde{\theta}) \tag{2.7}$$

which has a derivative

$$\begin{aligned} \dot{V} =& e^T(A_m^T P + PA_m)e + 2e^T Pe\tilde{\theta}x + 2\ Trace(\dot{\tilde{\theta}}^T\ \Gamma^{-1}\ \tilde{\theta}) \\ =& -e^T Qe + 2e^T PeB_m\tilde{\theta}x - 2\ Trace(x\ e^T PB_m\tilde{\theta}) \\ =& -e^T Qe \leq 0 \end{aligned} \tag{2.8}$$

where $\tilde{\theta} = \theta - \theta^*$. In proving (2.8), we have used the matrix identity $Trace(ab^T) = b^T a$ for column vectors a and b.

Remark 1 : A small perturbation of the assumption in (2.2) has been used extensively in the design of adaptive flight control systems [13]. This corresponds to an assumption that B is unknown but is such that

$$B\Lambda^* = B_m \tag{2.9}$$

where B_m is known and Λ^* is a *diagonal* matrix with the signs of its diagonal elements known. Such an assumption is quite reasonable in problems where uncertainties occur due to anomalies in actuators [13],[14].

Stability Proof : The corresponding Lyapunov function for this case is

$$V = e^T Pe + Trace(|\Lambda^*|\tilde{\theta}\ \Gamma^{-1}\ \tilde{\theta}^T) \tag{2.10}$$

It can be shown that (2.10) has a derivative

$$\dot{V} = -e^T Qe \leq 0$$

if the control law is chosen as

$$u = \theta x \tag{2.11}$$

$$\dot{\theta} = -sgn(\Lambda^*) B_m^T P e x^T \Gamma \tag{2.12}$$

where P satisfies (2.6), sgn denotes the sign function and

$$sgn(\Lambda^*) = diag(sgn(\lambda_1), sgn(\lambda_2), ..., sgn(\lambda_n)) \tag{2.13}$$

2.1.2 Unknown B

The problem is particularly more complex when B is unknown. The stability result that can be obtained differs drastically from that in the above section [4]. Since B is unknown, it is no longer possible to choose B_m of the reference model as $B_m = B$. The design of the controller requires an additional assumption that a non-singular matrix K^* exists such that

$$BK^* = B_m, \tag{2.14}$$

where B_m is known. The controller in this case is of the form

$$u = K\theta x \tag{2.15}$$

This yields an overall system described by,

$$\dot{x} = (A + BK\theta)x \tag{2.16}$$

Due to the structure of the control input in (2.15), assumption (2.2) is modified as

$$A + BK^*\theta^* = A_m \tag{2.17}$$

The error dynamics in this case can be written as

$$\begin{aligned}\dot{e} &= A_m e + [A + B(K^* + K - K^*)\theta - A_m]x \\ &= A_m e + B_m(\theta - \theta^*)x + B_m[K^{*-1}K - I]\theta x \\ &= A_m e + B_m\tilde{\theta}(t)x + B_m\tilde{\Psi}(t)u\end{aligned} \tag{2.18}$$

where,

$$\tilde{\theta}(t) = \theta(t) - \theta^* \tag{2.19}$$

$$\tilde{\Psi}(t) = K^{*-1} - K^{-1}(t) \tag{2.20}$$

It can be easily shown that

$$V = e^T P e + Trace(\tilde{\theta}^T\ \Gamma_\theta^{-1}\tilde{\theta} + \tilde{\Psi}^T\ \Gamma_\Psi^{-1}\tilde{\Psi}) \tag{2.21}$$

is a Lyapunov function of the system with a time derivative

$$\dot{V} = -e^T Q e \leq 0$$

if the control parameters are adjusted as,

$$\dot{\theta} = -\Gamma_\theta B_m^T P e x^T \tag{2.22}$$

$$\dot{K} = -\Gamma_\Psi K B_m^T P e u^T K \tag{2.23}$$

where e and x_m are defined as in (2.5) and P satisfies (2.6). The main point to note here is that in this case, the stability result is local. This occurs because the Lyapunov function assures global stability in the $\{e, \tilde{\theta}, \tilde{\Psi}\}$ space. Though the adaptive law ensures the boundedness of

$$\tilde{\Psi}(t) = K^{*-1} - K^{-1}(t)$$

the parameter of interest is

$$\tilde{K}(t) = K(t) - K^*(t).$$

As the Lyapunov function in $\{e, \tilde{\theta}, \tilde{K}\}$ space is *not* radially unbounded, the stability result is only *local* and not global.

2.2 Adaptive controller for systems with partially known input matrix B

The question that is raised by the discussions above is that can the local stability result be avoided, if additional information regarding B is known. We note that (2.14) can be equivalently expressed as

$$B = B_m \Psi^*. \tag{2.24}$$

Equation (2.24) implies that B_m lies in the subspace spanned by the columns of B. We assume that further information is available about Ψ^* as follows.

Assumption : *Let Ψ^* be such that there exists a sign-definite matrix M and a* known *symmetric positive-definite matrix Γ_0 such that*

$$\Gamma_0 \Psi^* + \Psi^{*T} \Gamma_0 = M \tag{2.25}$$

Equation (2.25) essentially implies that partial information is available regarding B such that a known B_m and a Ψ^* that satisfies a sign-definite condition exist. It should be noted that the class of such Bs satisfying (2.25) is quite larger than those satisfying (2.9). The assumption in (2.25) mainly allows us to find a globally stabilizing adaptive controller by not introducing the time-varying parameter K in (2.15). In the following, we show that if B is unknown but satisfies (2.24) and (2.25), a globally stabilizing adaptive controller can be derived.

We choose an adaptive controller of the form,

$$\begin{aligned} u &= \theta(t)x \\ \dot{\theta} &= -\Gamma B_m^T Pex^T, \quad \Gamma = \gamma\Gamma_0, \gamma > 0 \end{aligned} \tag{2.26}$$

The main stability result is stated and proved in Theorem below.

Theorem : *Under assumption* (2.2), (2.24) *and* (2.25), *the controller in* (2.26) *ensures that the plant in* (2.1) *can be globally stabilized and that*

$$\lim_{t\to\infty} x(t) = 0 \tag{2.27}$$

where P satisfies (2.6).

Proof : Using (2.2) and (2.24), we write the closed loop system equations as,

$$\dot{x} = (A + B\theta^*)x + B_m\Psi^*\tilde{\theta}x \tag{2.28}$$

leading to the error equation,

$$\dot{e} = A_m e + B_m\Psi^*\tilde{\theta}x \tag{2.29}$$

A Lyapunov function candidate,

$$V = e^T Pe + Trace(\tilde{\theta}^T(\Psi^{*T}\Gamma)\tilde{\theta}) \tag{2.30}$$

results in

$$\begin{aligned} \dot{V} =& e^T(A_m^T P + PA_m)e + e^T PB_m\Psi^*\tilde{\theta}x + x^T\tilde{\theta}^T\Psi^{*T}B_m^T Pe \\ &- Tr(\tilde{\theta}^T \ \Psi^{*T}\Gamma \ \dot{\tilde{\theta}}) - Tr(\dot{\tilde{\theta}} \ \Gamma\Psi^{*T} \ \tilde{\theta}) \\ =& - e^T Qe \leq 0 \end{aligned} \tag{2.31}$$

if the adaptive law is chosen as

$$\dot{\tilde{\theta}} = -\Gamma B_m^T P e x^T \tag{2.32}$$

and Γ satisfies assumption (2.25). This implies that the closed loop system is globally stable and e is bounded. A straight forward application of Barbalat's lemma results in,

$$\lim_{t \to \infty} e(t) = \lim_{t \to \infty} x(t) = 0 \tag{2.33}$$

2.2.1 $B = \Lambda B_p$: Uncertainties in plant dynamics

In this section we address the case of multiplicative uncertainties in B that occur due to changes in the plant dynamics. Let the control matrix B be of the form

$$B = \Lambda B_p \tag{2.34}$$

where $B_p \in \Re^{n x m}, n \geq m$ is known and is full rank and Λ is unknown. It is easy to show that assumption (2.25) is satisfied if Λ and B_p satisfy either of the following conditions,

(i) symmetric part of Λ is sign-definite

(ii) symmetric part of $B_p^T \Lambda B_p$ is sign-definite

In both cases, it can be shown that an M exists that satisfies (2.25) if $B_m = B_p$ and $\Gamma_0 = B_p^T B_p$. If condition (i) is true, then M exists for any full rank matrix B_p. However if Λ is not sign-definite, then B_p and Λ together should satisfy condition (ii).

Proof : For $B_m = B_p$, (2.24) can be written as,

$$\bar{\Lambda} B_p = B_p \Psi^* \tag{2.35}$$

$$\Rightarrow B_p^T \bar{\Lambda} B_p = B_p^T B_p \Psi^* \tag{2.36}$$

$$\Rightarrow \underbrace{B_p^T B_p}_{\Gamma_0} \Psi^* + \Psi^{*T} \underbrace{B_p^T B_p}_{\Gamma_0} = \underbrace{B_p^T (\bar{\Lambda} + \bar{\Lambda}^T) B_p}_{M} \tag{2.37}$$

2.2.2 $B = B_p\Lambda$: Anomalies in actuators

Loss of actuator effectiveness can be modeled by a post-multiplicative uncertainty matrix $\bar{\Lambda}$. The control matrix B is still unknown but is of the of the form

$$B = B_p \bar{\Lambda} \tag{2.38}$$

where $B_p \in \Re^{n \times m}$ is known and $\bar{\Lambda}$ is unknown. It is easy to show that assumption (2.25) is satisfied if

(i) symmetric part of Λ is sign-definite

In this case it can be easily shown that that an M exists that satisfies (2.25) if $B_m = B_p$ and $\Gamma_0 = I$.

Proof : For $B_m = B_p$, (2.24) can be written as,

$$B_p \bar{\Lambda} = B_p \Psi^* \tag{2.39}$$

$$\Rightarrow \bar{\Lambda} = \Psi^* \tag{2.40}$$

$$\Rightarrow \underbrace{I}_{\Gamma_0} \Psi^* + \Psi^{*T} \underbrace{I}_{\Gamma_0} = \underbrace{(\bar{\Lambda} + \bar{\Lambda}^T)}_{M} \tag{2.41}$$

It should be noted that the requirement of symmetric part of Λ to be sign-definite is much more general than that used in [13, 14], where $\bar{\Lambda}$ has to be diagonal and the sign of diagonal elements have to be known. Also the adaptive controller developed in this section allows for actuator anomalies which lead to coupling between different actuators (i.e. actuator responses are not independent of each other). Mathematically, the requirement that $\bar{\Lambda}$ is diagonal, tolerates uncertainties which only stretch the control subspace. However, assumption (2.25) allows the control subspace to both stretch and rotate as long as the rotation angle is acute (due to sign definiteness condition), thus allowing us to address a much larger class of problems.

Remark 2 : All the above discussions can be extended to the tracking problem where x_m is realized using a reference command r as

$$\dot{x}_m = A_m x_m + B_m r \tag{2.42}$$

by modifying u as

$$u = \theta(t)x + N(t)r \tag{2.43}$$

and suitably adapting N.

2.3 Adaptive Control with nonlinear damping

Control strategy using adaptive methods is to change the adaptive parameter θ based on the error between the plant and the reference model, e. If the plant is unstable, the error between the two is high initially and reduces with time,ultimately becoming zero. This high initial error can lead to a poor transient response. Though the transient response can be improved by using a large adaptive gain Γ, such a methodology usually leads to large control effort. The oscillatory nature in the transient response cannot be eliminated by just choosing a large gain.

Situations such as these are avoided by using a linear baseline controller (usually an LQR based controller) which stabilizes the nominal system. The adaptive controller yields good performance even though there is uncertainty in the plant parameters as the perturbed plant is usually stable. However, in certain scenarios, small parametric uncertainties can lead to large changes in the plant dynamics, making the perturbed plant unstable. The adaptive controller, which is trying to now stabilize an unstable plant, usually becomes ineffective.

2.3.1 Illustrative scalar example

To motivate the problem, let us consider a scalar system with unstable dynamics,

$$\dot{x} = ax + u, \qquad a = 3 \tag{2.44}$$

Let the objective of the controller be to track the reference model,

$$\dot{x}_m = a_m x_m + r, \qquad a_m = -1 \tag{2.45}$$

If the adaptive controller is of form $u = \theta x + r$, the adaptive law can be easily derived to be,

$$\dot{\theta} = -\gamma e x \tag{2.46}$$

Figure 2-1 shows the state, control and adaptive parameter response of the system to a unit step reference command for adaptive gains $\gamma = 1, 10$. As it can be easily seen, the transient response of the system is unsatisfactory. The initial control effort is also very large.

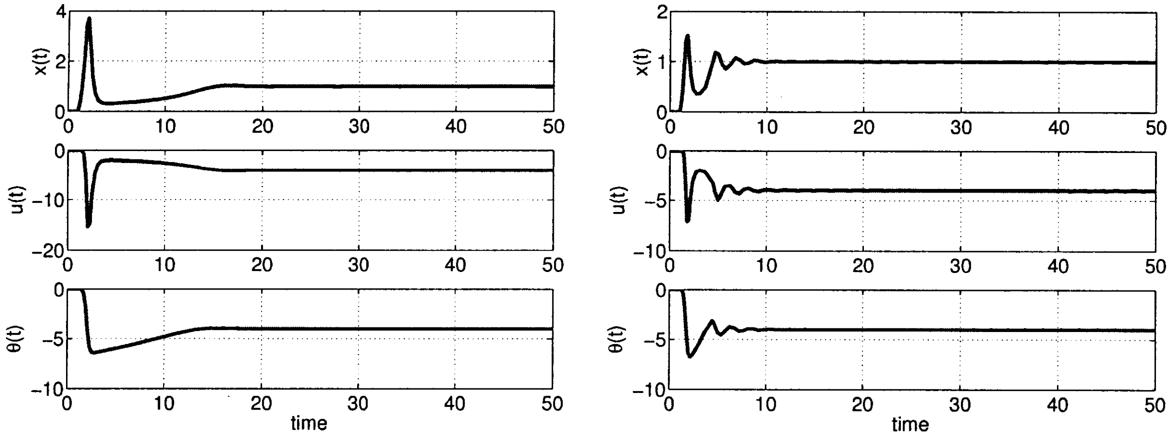

(a) (b)

Figure 2-1: System response for nominal adaptive control with adaptive gains (a) $\gamma = 1$ and (b) $\gamma = 10$

The above problem can be solved in an effective manner by introducing the rate feedback of the adaptive parameter. The control input is now modified as

$$u = \theta x + K_D \dot{\theta} x + r \tag{2.47}$$

As the adaptive parameter $\dot{\theta}$ is a nonlinear function of the error and the state, augmenting the extra term adds nonlinear damping as,

$$u = \theta x - \gamma K_D e x^2 \tag{2.48}$$

Figure 2-2 shows the system response with derivative feedback. It should be noted that even for a small derivative gain $K_D = 1$, the transient response shows tremendous improvement.

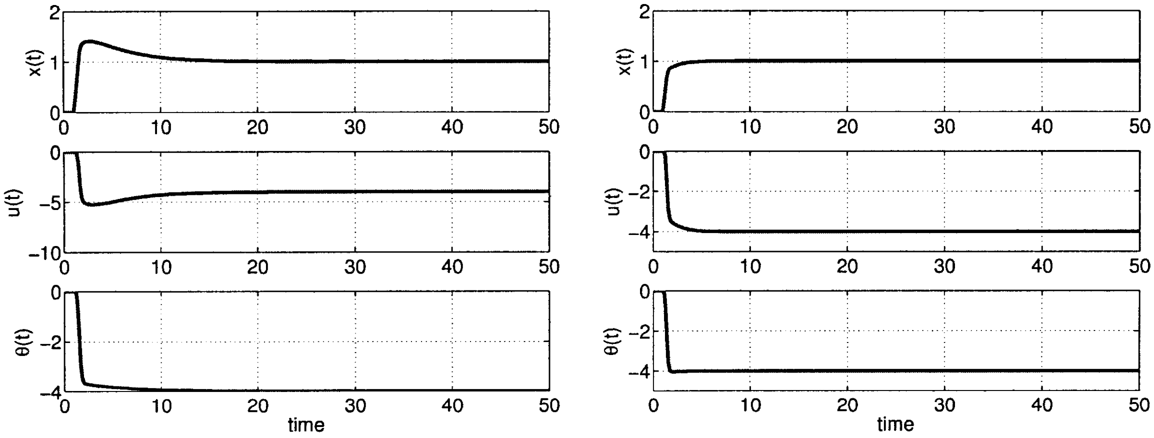

(a) (b)

Figure 2-2: System response for adaptive control with nonlinear damping with adaptive gains (a) $\gamma = 1$ and (b) $\gamma = 10$

2.3.2 Stability proof

Consider the MIMO plant with dynamics,

$$\dot{x} = Ax + Bu \tag{2.49}$$

where B is known. Let the objective of the adaptive controller of the form

$$u = \theta x + K_D \dot{\theta} x + r \tag{2.50}$$

where $K_D > 0$, be to track the reference model given by,

$$\dot{x}_m = A_m x_m + B_m r \tag{2.51}$$

Let there exist a known A_m and a θ^* such that

$$A + B\theta^* = A_m \tag{2.52}$$

The error dynamics with derivative control with $B_m = B$ is,

$$\dot{e} \;=\; A_m e + B_m \tilde{\theta} x + B_m \dot{\tilde{\theta}} \tag{2.53}$$

It can be easily shown that

$$V = e^T P e + Trace(\tilde{\theta}^T \Gamma^{-1} \tilde{\theta}) \tag{2.54}$$

is a Lyapunov function of the system with a time derivative,

$$\dot{V} \;=\; -e^T Q e - (e^T P B_m)^T K_D (e^T P B_m) \leq 0 \tag{2.55}$$

The nonlinear damping term makes $\dot{V}$ more negative and hence is able to improve transient performance as compared to the nominal adaptive controller.

Chapter 3

Modeling the HSV

A schematic of the HSV is shown in Figure 3-1. There are three control inputs for this vehicle, the elevator deflection δ_e, the canard deflection δ_c, and the equivalence ratio for the fuel in the scramjet ϕ. The canard has been added in recent studies in order to increase the available bandwidth for the control designs [15, 16]. However, due to harsh operating conditions experienced by the fore-body of the HSV, it might not be physically possible to realize the canard as a control input. For this reason, we assume that only elevator deflection and equivalence ratio are available as control inputs.

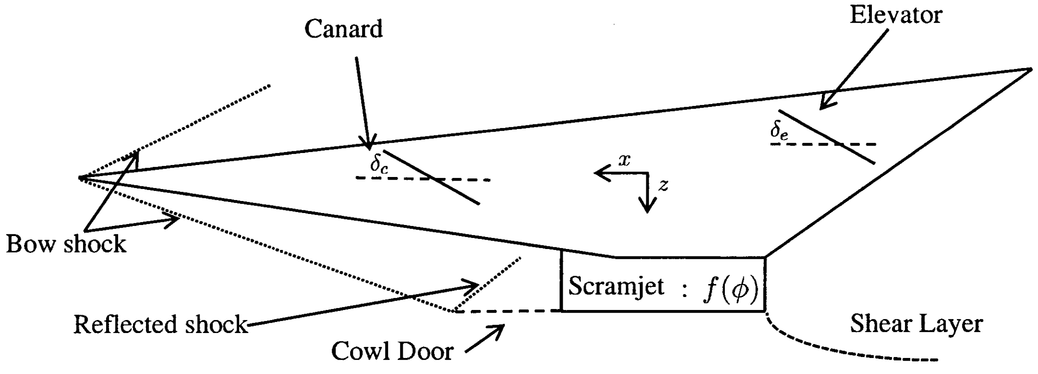

Figure 3-1: HSV side view I [17]

The research in vehicle modeling is mainly intended at developing a high fidelity model of the hypersonic vehicle which captures the effects of high speed aerodynamics, flexible dynamics and scramjet propulsion. Various models have been proposed in this regard. It should be noted that the current literature focuses on the longitudinal model of the HSV and assumes infinite lateral stiffness. This is a reasonable assumption for slender bodies for whom longitudinal dynamics govern stability and performance as compared to the lateral dynamics.

Hypersonic Aerodynamics : Earliest aerodynamic models used Newton impact theory to calculate the pressure distribution around the vehicle [18]. However, Newtonian theory was found to be inaccurate in predicting aerodynamic forces and moments. Piston theory was proposed by Oppenheimer [19] to model unsteady aerodynamics, but resulted in a complicated description, unsuitable for control design. Aerodynamic models which consider aerothermal [20] and viscous [21, 22] effects have been considered in the past. Lately, researchers have been increasingly using Oblique shock and Prandtl-Meyer expansion theory [17, 23, 24] as it provides an accurate yet simple model of the underlying aerodynamics.

Elastic Effects : Two main approaches have been used thus far to model elastic effects of the HSV. The first approach proposed by Bolender and Doman [17] models the HSV as double cantilever beam fixed at the center of gravity. A Lagrangian approach was used to develop the dynamical model of the HSV from first principles. The vehicle model thus developed predicted direct coupling between the elastic modes and the pitching moment, which was later deemed unrealistic as it failed to match experimental results. Bilimoria and Schmidt [25, 26] modeled the HSV as a free-free beam and used assumed modes method to model flexible effects. The model used to validate control design uses this well known classical approach.

Propulsion Model : A simplified scramjet engine model was described by Chavez and Schmidt [27]and has remained the central approach to model scramjet engines in the context of HSV till date. The engine was modeled as a 1-D duct and an isentropic flow was assumed. The main contribution of their work was the development of an analytical relationship that predicted pressure distribution at the aft of the nozzle, enabling one to calculate the thrust generated by the scramjet engine. An engine model that includes effects of pre-combustion shocks and dissociation has been proposed by [28, 29]. Though this model explicitly accounts for chemical reactions inside the combustion chamber, it fails to provide an input output relationship needed for control design.

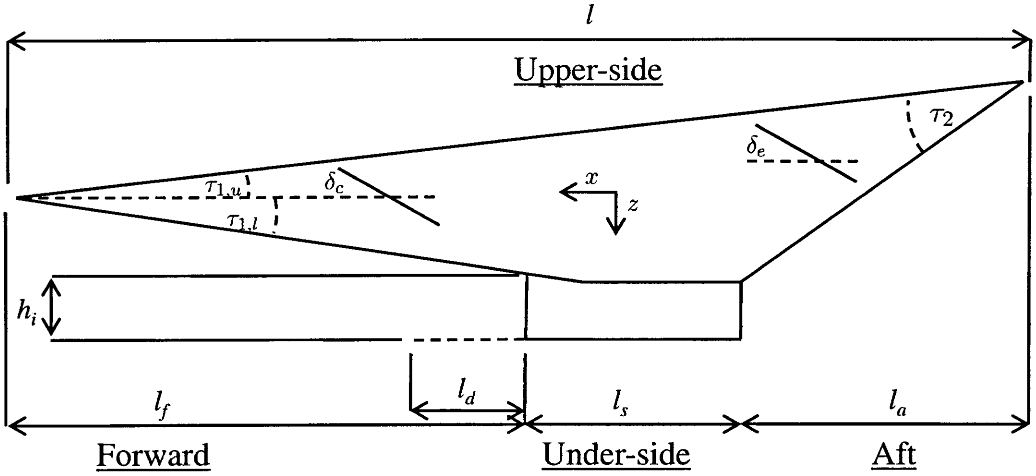

l
Upper-side
$\tau_{1,u}$
$\tau_{1,l}$
δ_c
x
z
δ_e
τ_2
h_i
l_f
l_d
l_s
l_a
Forward
Under-side
Aft

Figure 3-2: HSV side view II [17]

3.1 Rigid Body Model

When a supersonic flow is turned onto itself, an oblique shock is generated [30] (Fig 3-3). The flow after passing through the shock is turned parallel to inclined surface. The shock angle θ_s is a function of the wedge angle δ,

$$\sin^6\theta_s + b\sin^4\theta_s + c\sin^2\theta_s + d = 0 \tag{3.1}$$

where

$$b = -\frac{M_1^2+2}{M_1^2} - \gamma\sin^2\delta \tag{3.2}$$

$$c = \frac{2M_1^2+1}{M_1^4} + \left[\frac{(\gamma+1)^2}{4} + \frac{\gamma-1}{M_1^2}\right]\sin^2\delta \tag{3.3}$$

$$d = -\frac{\cos^2\delta}{M_1^4} \tag{3.4}$$

Here M denotes the Mach number and γ is the ratio of specific heats ($\gamma = C_p/C_v$).

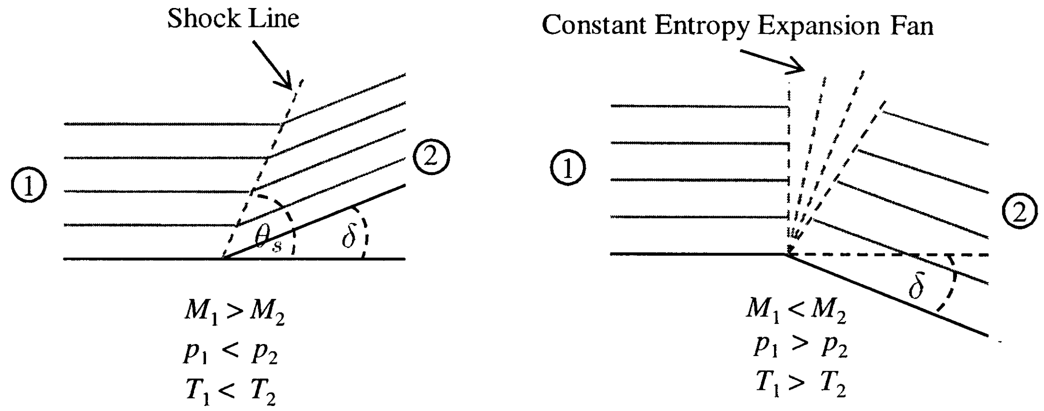

Oblique Shock Theory

Prandtl-Meyer Expansion

Figure 3-3: Oblique shock and Prandtl-Meyer expansion theory[30]

Subscripts 1 and 2 denote the flow properties before and after the shock. The post shock flow properties, namely the pressure p, temperature T, and Mach number M, can then be obtained using the following relations [30] ,

$$\frac{p_2}{p_1} = \frac{7M_1^2 \sin^2\theta_s - 1}{6} \tag{3.5}$$

$$\frac{T_2}{T_1} = \frac{\left(7M_1^2 \sin^2\theta_s - 1\right)\left(M_1^2 \sin^2\theta_s + 5\right)}{36M_1^2 \sin\theta_s} \tag{3.6}$$

$$M_2^2 \sin^2(\theta_s - \delta) = \frac{M_1^2 \sin^2\theta_s + 5}{7M_1^2 \sin^2\theta_s - 1}. \tag{3.7}$$

However, if the flow is turned around a corner, a Prandtl-Meyer expansion fan is created. The flow expands isentropically until it becomes parallel to the inclined edge. The flow properties after the expansion are a function of the turn angle δ and the incoming flow Mach number M_1,

$$\delta = \nu(M_2) - \nu(M_1) \tag{3.8}$$

where

$$\nu(M) = \sqrt{\frac{\gamma+1}{\gamma-1}} \arctan\Big(\sqrt{\frac{\gamma+1}{\gamma-1}(M^2-1)}\Big) \arctan(\sqrt{M^2-1}) \tag{3.9}$$

is the Prandtl-Meyer expansion function. Post expansion flow properties can be calculated as [30],

$$\frac{p_2}{p_1} = \left[\frac{1+[(\gamma-1)/2]M_1^2}{1+[(\gamma-1)/2]M_2^2}\right]^{\gamma/(\gamma-1)} \tag{3.10}$$

$$\frac{T_2}{T_1} = \frac{1+[(\gamma-1)/2]M_1^2}{1+[(\gamma-1)/2]M_2^2}. \tag{3.11}$$

Given the geometry of the HSV and the upstream Mach number M_∞, pressure distribution over the vehicle can be directly calculated. Forces and moments can be obtained by integrating the pressure over the vehicle area. The same approach is used for evaluating forces and moments generated due to elevator deflection and at the inlet of the scramjet engine.

3.2 Propulsion Model

The propulsion model described here is based on the work done by Chavez and Schmidt [27]. The scramjet engine is modeled as 1-D duct in isentropic flow. A schematic of the scramjet is shown in Figure 3-4. The scramjet engine has three parts; the diffuser (or compressor), the combustion chamber and the nozzle. The model assumes isentropic compression of the flow in the diffuser, constant area heat addition in the combustion chamber and an isentropic expansion in the nozzle. The flow properties at the inlet of the diffuser can be calculated using oblique shock theory, given the free stream Mach number. The Mach number of the flow at the exit of

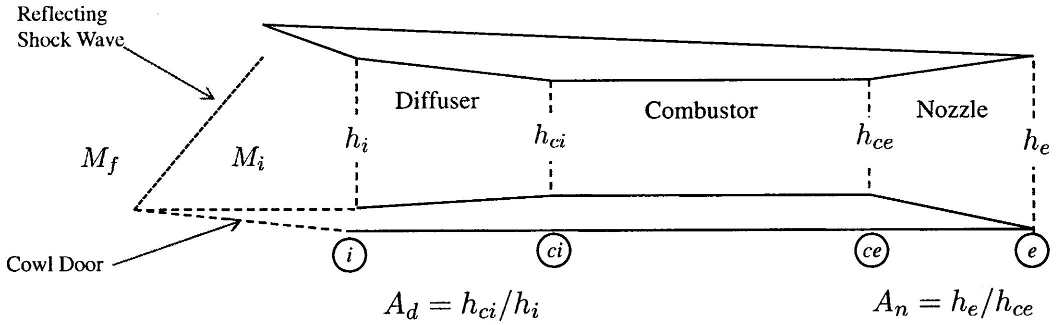

Figure 3-4: Schematic of Scramjet Engine [17, 27]

the diffuser is given by,

$$\frac{\left[1+[(\gamma-1)/2]M_{ci}^2\right]^{(\gamma+1)/(\gamma-1)}}{M_{ci}^2} = A_d^2\frac{\left[1+[(\gamma-1)/2]M_i^2\right]^{(\gamma+1)/(\gamma-1)}}{M_i^2} \tag{3.12}$$

where subscripts $(\cdot)_i$ and $(\cdot)_{ci}$ denote the flow properties at the inlet to the diffuser and that to the combustor respectively. A_d is the diffuser area ratio. Pressure and temperature of the flow at the inlet of the combustor can be calculated using equations (3.10) and (3.11).

The Mach number at the combustor exit M_{ce} is a function of the total temperature change across the combustor ΔT_{t_c} due to heat addition,

$$\frac{M_{ce}^2\left[1+[(\gamma-1)/2]M_{ce}^2\right]}{(\gamma M_{ce}^2+1)^2} = \frac{M_{ci}^2\left[1+[(\gamma-1)/2]M_{ci}^2\right]}{(\gamma M_{ci}^2+1)^2} + \frac{M_{ci}^2}{(\gamma M_{ci}^2+1)^2}\frac{\Delta T_{t_c}}{T_{ci}} \tag{3.13}$$

The temperature and pressure at the combustor exit can then be calculated using,

$$p_{ce} = p_{ci}\frac{1+\gamma M_{ci}^2}{1+\gamma M_{ce}^2} \tag{3.14}$$

$$T_{ce} = T_{ci}\left[\left(\frac{1+\gamma M_{ce}^2}{1+\gamma M_{ci}^2}\right)\frac{M_{ci}}{M_i}\right]^2 \tag{3.15}$$

The total temperature change across the combustor is a function of the equivalence ratio ϕ,

$$\frac{T_{t_{ce}}}{T_{t_{ci}}} = \frac{1+H_f\eta_c f_{st}\phi/(c_pT_{t_{ci}})}{1+f_{sT}\phi} \tag{3.16}$$

$$\Delta T_{t_c} = T_{t_{ce}} - T_{t_{ci}} \tag{3.17}$$

where η_c is the efficiency of the scramjet (0.9), f_{st} is the stoichiometric air-fuel ratio (0.0291), H_c is the heat of combustion for the fuel (LH2 at 51,500 BTU/lbm) and c_p is the specific heat of the fuel at constant pressure (0.24 BTU/(lbm°R) [17, 31, 32]. It should be noted that the total temperature and the static temperature have the following relationship,

$$\frac{T_t}{T} = 1 + \frac{\gamma - 1}{2} M^2. \tag{3.18}$$

The flow is isentropically expanded in the nozzle and the flow properties at the exit of the nozzle are given by,

$$\frac{\left[1 + [(\gamma - 1)/2] M_e^2\right]^{(\gamma+1)/(\gamma-1)}}{M_e^2} = A_n^2 \frac{\left[1 + [(\gamma - 1)/2] M_{ce}^2\right]^{(\gamma+1)/(\gamma-1)}}{M_{ce}^2} \tag{3.19}$$

where A_n is the area of the nozzle.

The flow coming out of the nozzle interacts with that turned by the upper body of the HSV, resulting in a shear layer. Chavez and Schmidt found an analytical expression for the pressure distribution at the aft of the scramjet engine as a function of free stream air pressure p_a,

$$p_a = \frac{p_e}{1 + s_a/l_a(p_e/p_\infty - 1)} \tag{3.20}$$

where l_a is the length of the aft of the aircraft in the x–body direction and s_a is the length coordinate in the x–body direction.

The total thrust generated by the scramjet engine can be calculated using conservation of momentum,

$$\mathcal{T} = \dot{m}_a(V_e - V_\infty) + (p_e - p_\infty)h_e - (p_i - p_\infty)h_i. \tag{3.21}$$

The forces and moments generated due to scramjet engine can be calculated once the pressure distribution around the engine is known. Similar analysis can be done for the forces and moments generated due to the elevator deflection. Depending on the angle of attack and the elevator deflection, one face of the elevator generates an oblique shock and other an expansion fan. The difference in the pressures gives the lift force. The pitching moment can be calculated given the location of the elevator with respect to the center of gravity.

The total force and moment on the HSV in the longitudinal plane can thus be calculated by summing up individual contributions from the upper-body (u), lower fore-body (f), scramjet engine (s) and the elevator (e) ,

$$F_x = F_{x,u} + F_{x,f} + F_{x,s} + F_{x,e} \tag{3.22}$$

$$F_z = F_{z,u} + F_{z,f} + F_{z,s} + F_{z,e} \tag{3.23}$$

$$M_y = M_{y,u} + M_{y,f} + M_{y,s} + M_{y,e} + z_{\mathcal{T}}\mathcal{T}. \tag{3.24}$$

where $\mathcal{T}$ denotes the thrust and $z_{\mathcal{T}}$ denotes the vertical location of the scramjet engine with respect to the center of gravity of the HSV.

3.3 Elastic Model

The elastic effects are obtained by modeling the HSV as a free-free Euler-Bernouli Beam as shown in Figure 3-5. Let the beam be subjected to a time varying distributed load $f(x,t)$. The displacement y(x,t) of the HSV can be approximated by a finite series,

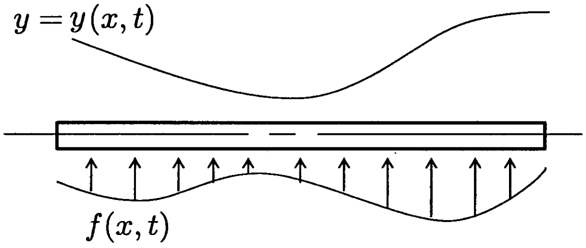

Figure 3-5: Assumed Modes Method

$$y(x,t) = \sum_{i=1}^{n} \phi_i(x) q_i(t) \tag{3.25}$$

where $\phi_i(x)$ are known trial functions and $q_i(t)$ are unknown generalized co-ordinates [33]. If we assume that there are no lumped mass at the boundaries, then the kinetic energy can be discretized as,

$$T(t) = \frac{1}{2}\int_0^L m(x)\dot{y}^2(x,t)dt \tag{3.26}$$

$$= \frac{1}{2}\sum_{i=1}^{n}\sum_{j=1}^{n} m_{ij}\dot{q}_i(t)\dot{q}_j(t) \tag{3.27}$$

where,

$$m_{ij} = \int_0^L m(x)\phi_i(x)\phi_i(j)dx, \quad i,j = 1,2,...,n \tag{3.28}$$

are symmetric mass co-efficients. The potential energy of the system can be similarly discretized as,

$$V(t) = \frac{1}{2}\int_0^L EI(x)[\frac{\partial^2 y(x,t)}{\partial x^2}]^2 dx \tag{3.29}$$

$$= \frac{1}{2}\sum_{i=1}^{n}\sum_{j=1}^{n} k_{ij}q_i(t)q_j(t) \tag{3.30}$$

where,

$$k_{ij} = \int_0^L EI(x)\frac{d^2\phi_i(x)}{dx^2}\frac{d^2\phi_j(x)}{dx^2}dx, \quad i,j = 1,2,...,n \tag{3.31}$$

are the symmetric stiffness co-efficients.

Finally, letting $f(x,t)$ to be a distributed non-conservative force, the virtual work can be discretized as follows,

$$\delta\bar{W} = \sum_{i=1}^{n} F(t)\delta q_i(t) \tag{3.32}$$

where,

$$F(t) = \int_0^L f(x,t)\phi_i(x)dx, \quad i = 1,2,...,n \tag{3.33}$$

The Lagrange's equation have the form,

$$\frac{d}{dt}\left(\frac{\partial T}{\partial \dot{q}_k}\right) - \frac{\partial T}{\partial q_k} + \frac{\partial V}{\partial q_k} = F_k, \quad k = 1, 2, .., n \tag{3.34}$$

Equating the forces we get,

$$\sum_{j=1}^{n} m_{ij}\ddot{q}_j(t) + \sum_{j=1}^{n} k_{ij}q_j(t) = F_i(t), \quad i = 1, 2, ..., n \tag{3.35}$$

which is nothing but the equations of motion of an -degree of freedom undamped system.

The trial functions $\phi_i(x)$ can be chosen from the admissible class of functions which satisfy the boundary conditions of a free-free beam. For the HSV, $f(x,t)$ is the pressure distribution per unit area. In the literature, usually three admissible bending modes have been used to model the flexible modes of the HSV [5].

3.4 Equations of Motion

Though the models developed above accurately predict forces and moments on the HSV, using them for validating control designs is computationally intensive. To facilitate ease and rapid evaluation of control designs, Parker et al. [16] suggested a control oriented model of the HSV. The main idea behind their work was to curve fit the forces and moments of the HSV into the well known rigid body aircraft model for the entire flight envelope. Flexible dynamics were augmented to this model to account for elastic effects. The work by Parker used the double cantilever beam model of Bolender and Doman[17]. This model was later found to be unrealistic as the predictions of the model did not match with that observed in flight tests. Fiorentini et al [5, 23, 24] used a free-free elastic beam model similar to that used by Bilimoria and Schmidt [25] to obtain the curve fit relationship. Three bending modes of the fuselage were considered to represent the flexible effects. The control designs developed in this thesis have been evaluated on the nonlinear model described in [5].

The details of the model are described below.

The equations of motion of the HSV consist of 5 rigid states and 6 elastic states, $\mathbf{x} = [V, \alpha, Q, h, \theta]^T$ and $\eta = [\eta_1, \dot{\eta}_1, \eta_2, \dot{\eta}_2, \eta_3, \dot{\eta}_3]^T$, where the rigid states are the velocity, angle of attack, pitch rate, altitude and pitch angle respectively, and the flexible states correspond to the three bending modes of the aircraft. The control inputs are elevator deflection (δ_e) and the equivalence ratio (ϕ) of the scramjet engine. The combined equations of motion are ([5]),

$$\dot{V} = (T\cos\alpha - D)/m - g\sin(\theta - \alpha) \tag{3.36}$$

$$\dot{\alpha} = -(T\sin\alpha + L)/mV + Q + (g/mV)\cos(\theta - \alpha) \tag{3.37}$$

$$\dot{Q} = M/I_{yy} \tag{3.38}$$

$$\dot{h} = V\sin(\theta - \alpha) \tag{3.39}$$

$$\dot{\theta} = Q \tag{3.40}$$

$$\ddot{\eta}_i = -2\zeta\omega\dot{\eta}_i - \omega_i^2\eta_i + N_i, \qquad i = 1, 2, 3 \tag{3.41}$$

$$L = L(\mathbf{x}, \eta, \delta_e), D = D(\mathbf{x}, \eta, \delta_e), M = M(\mathbf{x}, \eta, \delta_e)$$

$$N = N(\mathbf{x}, \eta), T = T(\mathbf{x}, \eta, \phi)$$

where, L, D and T denote the lift, drag and thrust forces respectively. M denotes the pitching moment and N_i represents the generalized forces generated due to the three bending modes of the fuselage. Although there is no coupling of rigid and elastic states through the equations of motion, the elastic states are directly coupled with rigid states through forces and moments. The lift, drag, thrust and moment are explicit functions of both rigid and elastic states. The functional relationship between the states and the lift, drag and moment co-efficients are described below,

$$\begin{aligned}
C_L &= C_L^{\alpha}\alpha + C_L^{\delta_e}\delta_e + C_L^0 + C_L^{\eta_i}\eta_i \\
C_M &= C_M^{\alpha^2}\alpha^2 + C_M^{\alpha}\alpha + C_M^{\delta_e}\delta_e + C_M^0 + C_M^{\eta_i}\eta_i \\
C_D &= C_D^{\alpha^2}\alpha^2 + C_D^{\alpha}\alpha + C_D^{\delta_e^2}\delta_e^2 + C_D^{\delta_e}\delta_e + C_D^0 + C_D^{\eta_i}\eta_i \qquad (3.42) \\
C_T &= C_T^{\phi\alpha^3}\alpha^3 + C_T^{\phi\alpha^2}\alpha^2 + C_T^{\phi\alpha}\alpha + C_T^{\phi} + C_T^3\phi^3 + C_T^2\phi^2 + C_T^1\phi + C_T^0 + C_T^{\eta_i}\eta_i \\
C_{N_j} &= C_{N_j}^{\alpha}\alpha + C_{N_j}^{\delta_e}\delta_e + C_{N_j}^{\eta_i}\eta_i, \quad i,j = 1,2,3
\end{aligned}$$

It should be noted that it is impractical to measure the flexible states and use them for control design. Thus the controller design is carried out on the rigid-body model of the HSV obtained by neglecting flexible states in (3.42). However, the designed controller is evaluated on the full scale non-linear model of the HSV taking flexible effects into account.

Chapter 4

Nonlinear model for Center of Gravity Uncertainty

The equations of motion of a rigid body are usually written about the center of gravity (CG). However, if the center of gravity moves, the equations of motion get fundamentally altered. For aircrafts, the position of the center of gravity with respect to the aerodynamic center determines the trimming moment, the frequency of the short period mode and the vehicle stability. Subsonic aircrafts usually have their CG located ahead of the aerodynamic center for static stability. A forward movement of center of gravity usually makes the aircraft more stable but requires the tail to generate a larger moment to trim. Large trimming moments require greater elevator deflections, which leads to increased drag. A backward CG shift on the other hand tends to make the aircraft less stable but more maneuverable and controllable. However, high performance aircrafts like the hypersonic vehicle, have unstable short period modes due to constraints imposed by high speed aerodynamics and the operation requirements of the scramjet engine.

Scramjet powered hypersonic vehicles require sharp leading edges and long, shallow fore-bodies (typically small angle wedges, cones, or scoops) because they are part of the inlet system and must generate relatively weak shock waves to enhance engine efficiency. Vehicle aft-bodies are also long and shallow because they are part of the scramjet nozzle and must be so for the nozzle to operate efficiently and create balancing pitching moments for reasonable vehicle trim. Note that the under-slung location of the scramjet engine generates a nose up pitching moment. This type of geometric configuration naturally results in the CG lying aft of both the low-speed aerodynamic center and the high-speed center of pressure, the latter occurring roughly at the center of vehicle planform area. Unless massive ballast is used to shift the CG forward, the CG lying aft of the high-speed center of pressure results in an unstable configuration at hypersonic speeds. With effort (by adjusting the internal arrangement of propellant and systems, etc.) a designer might be able to get the CG to lie at or slightly forward of the hypersonic center of pressure, resulting in neutral to slightly positive stability at hypersonic speeds. Regardless, stability will almost always be a challenge at low speeds when the aerodynamic center migrates forward to approximately the quarter-chord of the overall vehicle mean aerodynamic chord.

It cannot be assumed in general that for a flexible aircraft, a forward movement of CG is stabilizing. The flexible geometry leads to direct coupling of the pitching moment and flexible states. In such a scenario, a movement of CG in any direction changes the pitching moment, which in turn can excite the flexible states and lead to undesirable effects. For rigid aircrafts, CG shifts are usually modeled by scaling the stability derivatives. However, for high speed flexible vehicles such linear approximations inaccurately model CG shifts. It is also impractical to measure structural deformations of the HSV and use them for control design. The controller designs should be thus robust to excitations in the flexible dynamics which occur due to CG movements or otherwise. Modifying stability derivatives to model CG shifts does not give insights into how the vehicle model gets changed when the CG moves and how can we accommodate for it through controller design.

For all the reasons discussed above, we develop a nonlinear model of the center of gravity movements from first principles. The equations of motion of the aircraft are written about a body fixed point. The rational behind such a choice is that even if the CG moves, the equations of motion remain the same. As it will be shown in subsequent sections, by linearizing such a model, the CG shifts can be represented as parametric uncertainties thus providing insights into control design. The nonlinear model is first derived assuming the aircraft is rigid. Flexible dynamics are then augmented to this nonlinear model to account for vehicle flexibilities. This approach is similar to that being followed in the current literature [5].

4.1 Nonlinear model for Center of Gravity shifts

In this section we derive the nonlinear center of gravity model from first principles. Let the reference frame be located at an arbitrary body fixed point. Let U,V and W denote the velocities of the body fixed point in x, y, z axes. Let Δx, Δy and Δz denote the location of center of gravity (CG) with respect to the body fixed point. Also let P, Q and R denote the angular rates about roll(x), pitch(y) and yaw(z) axes respectively. Further let I_{ij} denote the moment of inertia about $i-j$ axis. It can be shown that the generalized equations of motion written about a body fixed point is [12],

$$\begin{aligned}
\Sigma F_x &= m\big[\dot{U} + QW - RV - (Q^2+R^2)\Delta x && (4.1)\\
&\quad + (QP-\dot{R})\Delta y + (RP+\dot{Q})\Delta z + g\sin(\theta)\big] && (4.2)\\
\Sigma F_y &= m\big[\dot{V} + RU - PW + (PQ+\dot{R})\Delta x && (4.3)\\
&\quad - (P^2+R^2)\Delta y + (QR-\dot{P})\Delta z - g\cos(\theta)\sin(\phi)\big] && (4.4)\\
\Sigma F_z &= m\big[\dot{W} + PV - QU + (PQ-\dot{Q})\Delta x && (4.5)\\
&\quad + (QR+\dot{P})\Delta y - (P^2+Q^2)\Delta z - g\cos(\theta)\cos(\phi)\big] && (4.6)
\end{aligned}$$

$$\begin{aligned}
\Sigma M_x &= I_{xx}\dot{P} - I_{xy}\dot{Q} - I_{xz}\dot{R} + I_{xy}PR - I_{xz}PQ + (I_{zz}-I_{yy})QR + (R^2-Q^2)I_{yz} && (4.7)\\
&+ m\big[(PV - QU + \dot{W} - g\cos(\theta)\cos(\phi))\Delta y + (PW - RU - \dot{V} + g\cos(\theta)\sin(\phi))\Delta z\big] &&\\
\Sigma M_y &= -I_{xy}\dot{P} + I_{yy}\dot{Q} - I_{yz}\dot{R} + I_{yz}PQ - I_{xy}QR + (I_{xx}-I_{zz})PR + (P^2-R^2)I_{xz} && (4.8)\\
&+ m\big[(QU - PV - \dot{W} + g\cos(\theta)\cos(\phi))\Delta x + (QW - RV + \dot{U} + g\sin(\theta))\Delta z\big] &&\\
\Sigma M_z &= -I_{xz}\dot{P} - I_{yz}\dot{Q} + I_{zz}\dot{R} + I_{xz}QR - I_{yz}PR + (I_{yy}-I_{xx})PQ + (Q^2-P^2)I_{xy} && (4.9)\\
&+ m\big[(RU - PW + \dot{V} - g\cos(\theta)\sin(\phi))\Delta x + (RV - QW - \dot{U} - g\sin(\theta))\Delta y\big] &&
\end{aligned}$$

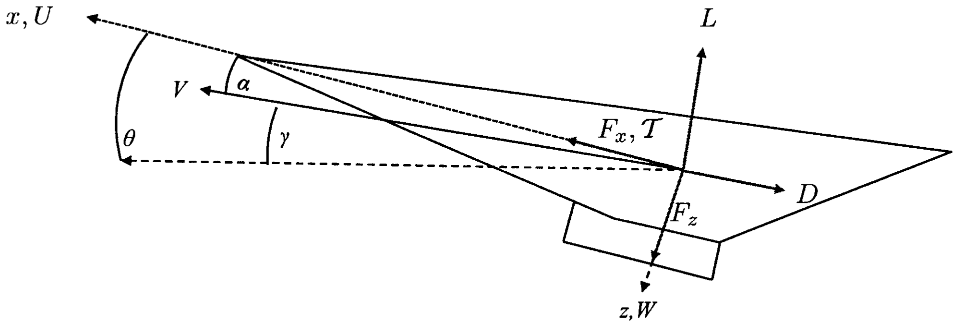

Figure 4-1: Axes of the HSV (from [8])

where F_x, F_y and F_z are the forces and M_x, M_y and M_z are the moments in the x, y and z axes respectively. To develop a longitudinal model, we assume that the motion of the HSV is limited to the x-z plane. The velocities and angular rates in the lateral direction are neglected.

$$V = 0, \quad \dot{V} = 0, \quad P = R = 0, \quad \dot{P} = \dot{R} = 0 \quad \phi = 0 \tag{4.10}$$

To be consistent with the longitudinal axis assumption, we should also assume that there is no lateral shift of CG, i.e $\Delta y = 0$. As the hypersonic vehicle is symmetric about the $x - z$ plane, the moment of inertias I_{xy} and I_{yz} are identically zero. Under these assumptions the equations of motion get simplified to,

$$\begin{aligned}
\Sigma F_x &= m\big[\dot{U} + QW - Q^2\Delta x + \dot{Q}\Delta z + g\sin(\theta)\big] && (4.11)\\
\Sigma F_y &= 0 && (4.12)\\
\Sigma F_z &= m\big[\dot{W} - QU + \dot{Q}\Delta x - Q^2\Delta z - g\cos(\theta)\big] && (4.13)\\
\Sigma M_y &= I_{yy}\dot{Q} + m\big[(QU - \dot{W} + g\cos(\theta))\Delta x \\
&\quad + (QW + \dot{U} + g\sin(\theta))\Delta z\big] && (4.14)
\end{aligned}$$

where, Δx, Δy and Δz denote the location of CG with respect to an arbitrary body fixed point. Fig 4-1 shows the body fixed axis system of the HSV. To develop a control oriented model and to simplify the equations of motion, we carry out a stability axis transformation. It should be noted that a more standard transformation of the co-ordinates by the angle of attack (α) defined by tan $\alpha = \frac{W}{U}$ is inappropriate, since by definition, the angle of attack is defined to be the angle that the velocity vector of the CG makes with the fuselage reference line.

The velocity at the center of gravity can be shown to be,

$$\begin{aligned} \mathbf{V_{cg}} &= \mathbf{V_{BF}} + \omega \times \bar{\rho} && (4.15) \\ &= (U + Q\Delta z - R\Delta y)\mathbf{i} + (V - P\Delta z + R\Delta x)\mathbf{j} \\ &+ (W + P\Delta y - Q\Delta x)\mathbf{k} && (4.16) \end{aligned}$$

where V_{cg} and V_{BF} denote the velocity vectors at the CG and body fixed point respectively. ω is the angular velocity vector and $\bar{\rho}$ is the position vector of the CG with respect to body fixed point.

Under the longitudinal dynamics assumption, the velocity at the center of mass simplifies to,

$$\mathbf{V_{cg}} = (U + Q\Delta z)\mathbf{i} + (W - Q\Delta x)\mathbf{k} \tag{4.17}$$

and the angle of attack, by definition is

$$\tan\alpha = \frac{W - Q\Delta x}{U + Q\Delta z} \tag{4.18}$$

If we define the total velocity at the center of mass as V, it can be shown that the following relations hold true,

$$V\cos\alpha = U + Q\Delta z \tag{4.19}$$

$$V\sin\alpha = W - Q\Delta x \tag{4.20}$$

$$\dot{V} = (\dot{U} + \dot{Q}\Delta z)\cos\alpha + (\dot{W} - \dot{Q}\Delta x)\sin\alpha \tag{4.21}$$

$$V\dot{\alpha} = (\dot{W} - \dot{Q}\Delta x)\cos\alpha - (\dot{U} + \dot{Q}\Delta z)\sin\alpha \tag{4.22}$$

A stability axis transformation consists of rotating the body fixed axis by the angle of attack in the counter-clockwise direction. The force equations get suitably modified,

$$F_{xS} = F_{xB}cos\alpha + F_{zB}sin\alpha \tag{4.23}$$

$$F_{zS} = -F_{xB}sin\alpha + F_{zB}cos\alpha \tag{4.24}$$

where subscript S denotes stability axes and B denotes body fixed axes respectively. Substituting the forces in the body-fixed axes from (4.11) and (4.13) and using (4.19) through (4.22), we get,

$$F_{xS} = m(\dot{V} + g\sin(\theta - \alpha)) \tag{4.25}$$

$$F_{zS} = m(V\dot{\alpha} - QV - g\cos(\theta - \alpha)) \tag{4.26}$$

Also the forces in the stability axes are given by,

$$F_{xS} = T\cos\alpha - D \tag{4.27}$$

$$F_{zS} = -(T\sin\alpha + L) \tag{4.28}$$

By balancing the forces we get,

$$\dot{V} = (T\cos\alpha - D)/m - g\sin(\theta - \alpha) \tag{4.29}$$

$$\dot{\alpha} = -(T\sin\alpha + L)/mV + Q + (g/mV)\cos(\theta - \alpha) \tag{4.30}$$

It should be noted that (4.29) and (4.30) are exactly same as (3.36) and (3.37), as though there has been no CG shift. However, the velocity predicted by these equations of motion is not that of body fixed point, but that of the new center of mass. If the moment equation is expressed in terms of the stability axes variables, then (3.38) gets modified to,

$$
\begin{aligned}
(I_{yy} - m(\Delta x^2 + \Delta z^2))\dot{Q} &= M \\
-m\big[\dot{V}(\Delta z\cos\alpha - \Delta x\sin\alpha) &- V\dot{\alpha}(\Delta x\cos\alpha + \Delta z\sin\alpha)\big] \\
&- mg(\Delta x\cos\alpha + \Delta z\sin\alpha)
\end{aligned} \tag{4.31}
$$

The above result is reasonable as a shift in the center of gravity does not change the lift produced but only brings about a change in the pitching moment. It should also be noted that a shift in CG changes the moment at trim.

4.2 Linearization

4.2.1 Linearized Model of the HSV

The design model described in (3.36)-(3.40) can be expressed compactly as a nonlinear model,

$$\dot{X} = f(X, U) \tag{4.32}$$

where $X = [V,\ \alpha,\ Q,\ h,\ \theta]^T$ is the state vector and $U = [\phi,\ \delta_e]^T$ is the control input. To facilitate control design, we linearize these equations about the trim state X_0 and trim input U_0 satisfying $f(X_0, U_0) = 0$ to obtain the following,

$$\dot{x} = A_p x + B_p u, \tag{4.33}$$

where,

$$A_p = \frac{\partial f}{\partial X}(X_0, U_0), \qquad B_p = \frac{\partial f}{\partial U}(X_0, U_0) \tag{4.34}$$

and x and u are perturbations about the trim point,

$$x = X - X_0, \qquad u = U - U_0 \tag{4.35}$$

Table 4.1: Variation of trim points as a function of CG movement

Δx (ft)	0	-0.5	0.5	-1	1
V (ft/s)	7850	7850	7850	7850	7850
α (rad)	0.0132	0.0129	0.0135	0.0126	0.0138
Q (rad/s)	0	0	0	0	0
h (ft)	85 000	85 000	85 000	85 000	85 000
θ (rad)	0.0132	0.0129	0.0135	0.0126	0.0138
δ_e (rad)	0.184	0.186	0.181	0.188	0.179
ϕ (-)	0.366	0.371	0.362	0.375	0.358

4.2.2 Effect of CG shift on dynamics

CG perturbations change the the nonlinear equations to

$$E(X)\dot{X} = f(X,U) + w(X) \tag{4.36}$$

where ,

$$w(X) = -mg(\Delta x \cos\alpha + \Delta z \sin\alpha) \tag{4.37}$$

The CG shift changes the equilibrium point from (X_0, U_0) to (X_0', U_0') due to presence of the additional term $w(X)$. Linearization about the new equilibrium point yields the following state and control matrices,

$$\bar{A}_p = E^{-1}(X_0')\frac{\partial(f+w)}{\partial X}(X_0', U_0') \tag{4.38}$$

$$\bar{B}_p = E^{-1}(X_0')\frac{\partial f}{\partial U}(X_0', U_0') \tag{4.39}$$

Table 4.1 shows the effect of CG shift, Δx on the trim condition. As it can be easily seen, small changes in CG do not bring about a drastic change in the trim condition. Thus, we make a reasonable assumption that trim conditions remain the same for small CG shifts. We further assume that the change in moment of inertia is small, $I = I_{yy} - m(\Delta x^2 + \Delta z^2) \sim I_{yy}$. It can be shown that CG uncertainty manifests itself in the linear system (4.33) as,

$$\dot{x} = \Lambda A_p x + \Lambda B_p u + D \tag{4.40}$$

where,

$$\Lambda = \begin{pmatrix} 1 & 0 & 0 & 0 & 0 \\ 0 & 1 & 0 & 0 & 0 \\ -P & R & 1 & 0 & 0 \\ 0 & 0 & 0 & 1 & 0 \\ 0 & 0 & 0 & 0 & 1 \end{pmatrix} \tag{4.41}$$

$$D = [0\ 0\ -d\ 0\ 0]^T \tag{4.42}$$

and,

$$P = \frac{m}{I}(\Delta z \cos\alpha - \Delta x \sin\alpha) \tag{4.43}$$

$$R = \frac{mV}{I}(\Delta x \cos\alpha + \Delta z \sin\alpha) \tag{4.44}$$

$$d = \frac{mg}{I}(-\Delta x \sin\alpha + \Delta z \cos\alpha) \tag{4.45}$$

An order of magnitude analysis for the uncertainties, P, R and d shows that R is the most prominent term. As the trim angle of attack α is usually close to zero, the uncertainty d can be neglected. It should be noted that as the magnitude of uncertainties depend on the mass, inertia and velocity of the vehicle, one uncertainty might be more prominent than others depending on the vehicle in question.

It should also be noted that a linear controller of the form $u = -Kx$ does not stabilize the perturbed plant dynamics (4.40), even though the gain K stabilizes (4.33). The next chapter will discuss how to design stabilizing adaptive controllers in presence of CG movements.

Chapter 5

Application to Hypersonic Vehicles

The tools developed thus far will be applied to the hypersonic vehicle in this chapter. The plant dynamics of the HSV consist of 5 rigid and 6 flexible states. The control inputs of the HSV are the elevator deflection and the equivalence ratio. As discussed earlier, the open loop dynamics of the HSV are unstable. Table 5 shows equilibrium points of the HSV, with the vehicle trimmed at 85 000 ft and Mach 8. The eigenvalues

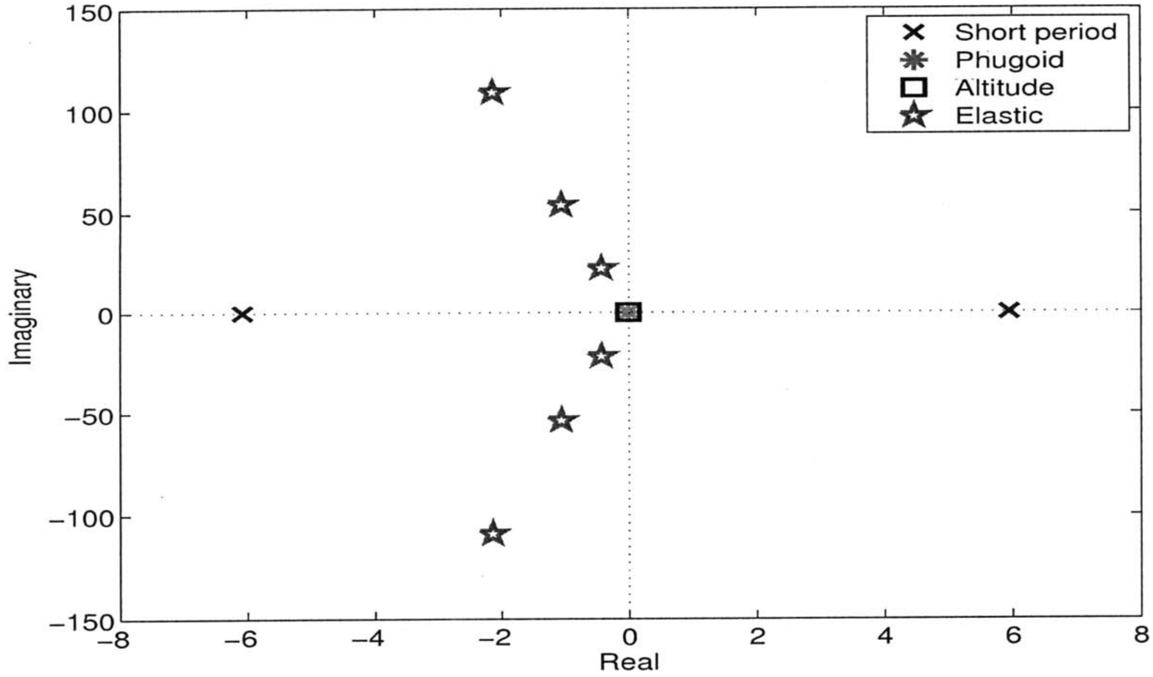

Figure 5-1: Eigenvalues of the HSV

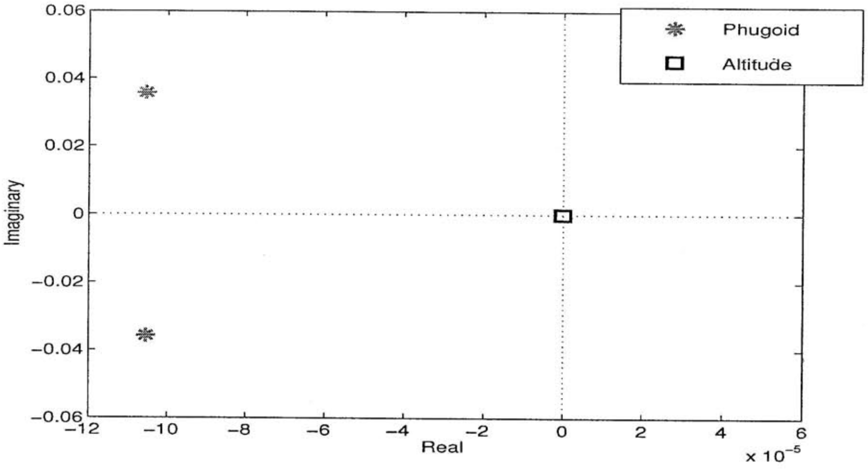

Figure 5-2: Altitude and Phugoid modes

of the plant at this trim condition are shown in Fig 5-1. It should be noted that one irregular short period mode of the HSV is in the right half plane, making the vehicle unstable. The phugoid and the altitude modes are very close to the origin and have been shown in Fig 5-2. The first three elastic modes of the fuselage of the HSV occur at high frequencies compared to the rigid body modes. Due to harsh operating conditions, uncertainties in the lift co-efficients can cause A_p to change as $A_p(\lambda)$. As discussed in earlier chapters, CG movements cause uncertainties both in A_p and B_p. Therefore the linear model in (4.40) takes the form (2.1) with

$$\Lambda A_p(\lambda) = A, \quad \Lambda B_p = B. \tag{5.1}$$

The D term has been neglected as we consider CG movements only along the x axis (Δx) and the angle of attack α is small. The nominal value control matrix B_p of the HSV is

$$B_p = \begin{pmatrix} 43.184 & -69.415 \\ 0 & -0.019428 \\ 0.70776 & -9.445 \\ 0 & 0 \\ 0 & 0 \end{pmatrix} \tag{5.2}$$

States	Trim Value	Units
V	7850	ft/s
α	0.0268	rad
q	0	rad/s
h	85000	ft
θ	0.0268	rad
η_1	1.08	–
$\dot{\eta}_1$	0	–
η_2	-0.079	–
$\dot{\eta}_2$	0	–
η_3	0	–
$\dot{\eta}_3$	0	–

Table 5.1: Trim values for HSV

where as the uncertainty matrix $\bar{\Lambda}$ for a CG shift of $\Delta_x = 1ft$ is,

$$\bar{\Lambda} = \begin{pmatrix} 1 & 0 & 0 & 0 & 0 \\ 0 & 1 & 0 & 0 & 0 \\ 0 & -15 & 1 & 0 & 0 \\ 0 & 0 & 0 & 1 & 0 \\ 0 & 0 & 0 & 0 & 1 \end{pmatrix} \tag{5.3}$$

It can be easily shown that eigenvalues of $B_p^{-1}\Lambda B_p$ are positive. By choosing $B_m = B_p$, it was found that a choice of $\Psi^* = B_p^{-1}\bar{\Lambda} B_p$ satisfied assumption (2.25) for a large range of CG perturbations in P and R in (4.43) and (4.44), thereby making the adaptive control design develop in Chapter 2 applicable.

5.1 Control Architecture

The goal of the control design is that the states $X_g = [V,\ h]^T$ follow a commanded trajectory $X_{g_c} = [V_c,\ h_c]^T$ that correspond to a desired flight envelope. The control task is therefore to ensure that $X_g(t)$ tracks $X_{g_c}(t)$ while the remaining states $X_p = [\alpha,\ \theta,\ ,Q]^T$ remain bounded. This command tracking task is converted into successive regulation around a family of trim points in the following manner.

A family of trim points $X_{g,i}, X_{p,i}, U_i,\ i = 1, 2, ..., N$ is obtained in the $V-h$ space

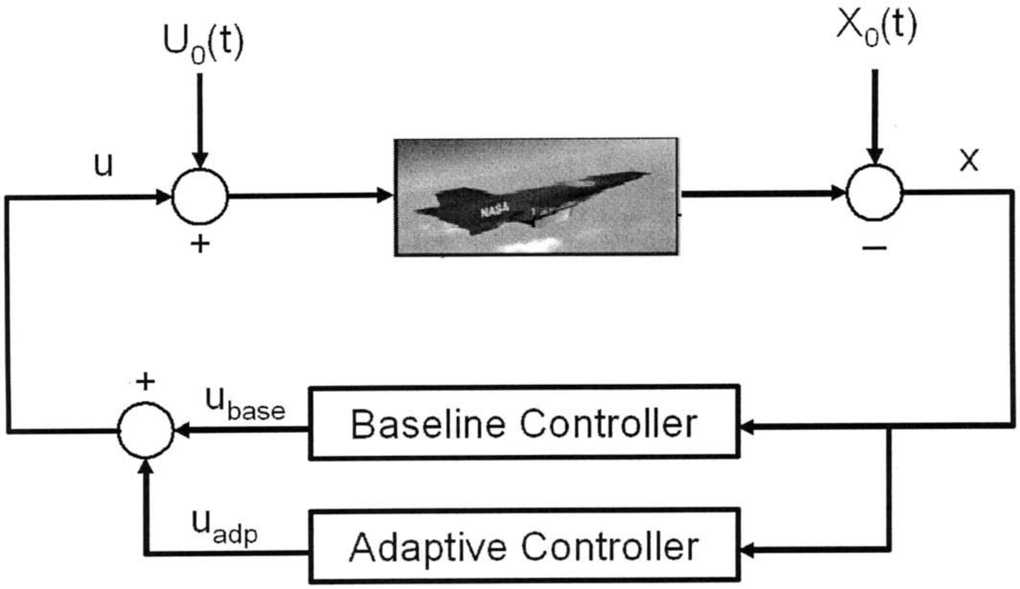

Figure 5-3: Adaptive Control Architecture

(see figure 5-4) such that they solve the nonlinear equation (4.32)

$$f(X_{g,i}, X_{p,i}, U_i) = 0, \quad i = 1, 2, ..., N \tag{5.4}$$

$$X_{p,i} = X_{p,i}(X_{g,i}), \quad U_i = U_i(X_{g,i}). \tag{5.5}$$

Using these trim points, a scheduled trim trajectory is obtained by interpolation as,

$$U_0(t) = U_i + M(X_{g,i}, X_{g_c}(t)) \tag{5.6}$$

$$X_{p0}(t) = X_{p,i} + M(X_{p,i}, X_{g_c}(t)) \tag{5.7}$$

$$X_{g0}(t) = X_{g,c}(0) \tag{5.8}$$

where M is an interpolation function. It can be shown that,

$$||f(X_{p0}(t), X_{g0}(t), U_0(t))|| \leq \epsilon,$$

where ϵ is arbitrary small [34]. Thus between two time intervals close to each other, the tracking problem becomes a regulation problem about a given trim point, making the controller designs developed in previous chapters applicable. Though the tracking

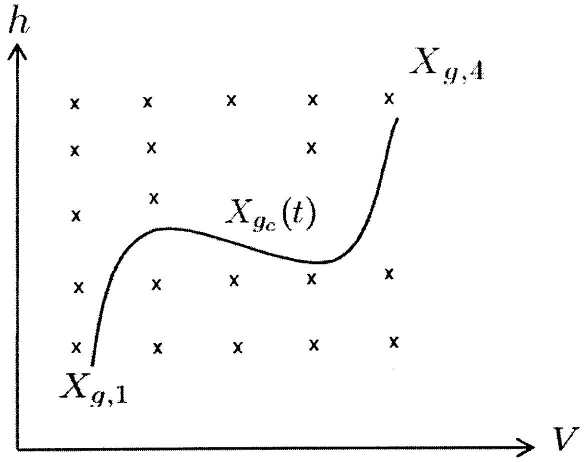

Figure 5-4: Trim trajectory

task has been solved by regulating the plant about the trim trajectories, it was found that gain-scheduling was not needed as the system matrices did not vary significantly with velocity and altitude. The adaptive control architecture is shown in fig 5-3. The control input $u(t)$ is a combination of a linear controller augmented with an adaptive component and can be represented as,

$$u(t) = u_{base} + u_{adp} \tag{5.9}$$

The proceeding sections show how each component is designed.

5.2 Linear Controller Design

The baseline controller is designed using the Linear Quadratic Regulator approach, so as to minimize the cost functional,

$$J = \int (x^T R_{xx} x + u^T R_{uu} u + \dot{x}^T S \dot{x}) dt, \tag{5.10}$$

where R_{xx} , R_{uu} and S are suitably chosen diagonal positive definite matrices, leading to a linear state feedback $u = -Kx$. It should be noted that the derivative of states have also been penalized in the cost function to gain control over the vehicle load factor. The structural requirements put a limit on the maximum permissible vehicle load factor. As the load factor is a function of vehicle acceleration, the weighting S gives direct control over the structural requirements.

As actuator saturation is important for controllers for high performance vehicles, we develop a strategy to maximize the initial condition set inside which control law does not saturate. Consider a linear SISO plant with dynamics,

$$\dot{x} = Ax + bu \tag{5.11}$$

Given that the initial conditions lie inside a certain ellipsoid, $x(0) \in x^T M x \leq \alpha$ $(M, \alpha > 0)$, the objective is to find the maximum value attained by the control input u. The problem can be represented as a Lagrange multiplier based optimization problem,

$$\begin{aligned} \mathbf{max} \quad & u = |Kx|, & (5.12) \\ s.t \quad & x^T M x \leq \alpha & (5.13) \end{aligned}$$

It can be easily shown that the maximum value of the control input u^* is attained at the boundary of the ellipsoid and is given by,

$$|u^*| = \sqrt{KM^{-1}K^T\alpha} \tag{5.14}$$

Let the saturation value of the control input be u_{max}. If the maximum value of control input is to remain less than the saturation value, $u^* < u_{max}$, then the bound on the radius of the ellipsoid should be,

$$\alpha < \frac{u_{max}^2}{KM^{-1}K^T} \tag{5.15}$$

Thus, in order to maximize the initial condition set, $KM^{-1}K^T$ has to be minimized. Note that if $M = I$, then the condition requires minimization of the L_2 norm of K.

The design methodology can be easily extended to MIMO systems noting that the plant dynamics can be written as,

$$\dot{x} = Ax + \sum_{i=1}^{m} b_i u_i \tag{5.16}$$

where $u_i, i = 1, 2, ..., m$ are the individual control inputs. Depending on the saturation limits on each control input, the individual norms of the control gains, $||K_i||_2$ should be minimized. It should be noted that the procedure does not yield a stabilizing controller on it own, but gives a method to choose the control gain that maximizes the stability domain under saturation.

5.3 Adaptive Controller Design

The second component is the adaptive controller and is chosen as,

$$u_{adp} = \theta x \tag{5.17}$$

$$\dot{\theta} = -\Gamma e^T P B_m x^T, \quad \Gamma = \gamma \Gamma_0, \gamma > 0 \tag{5.18}$$

where Γ_0 satisfies (2.25). Since the uncertainties in the HSV can be such that the plant is open loop unstable, another feature is added to the adaptive controller in the form of nonlinear damping. Traditionally employed for the control of higher relative degree plants [4], this addition introduces a term $\dot{\theta}x$ into the adaptive control input. As a result, the controller in (5.17) is modified as,

$$u_{adp} = \theta x + K_D \dot{\theta} x, \tag{5.19}$$

where the derivative gain, K_D is a diagonal positive definite matrix. The stability of the resulting system with the derivative term can be easily shown using (2.30) as the Lyapunov function whose time derivative is,

$$\dot{V} = -e^T Q e - (x^T x)(e^T P B_m)^T K_D M (e^T P B_m) \leq 0 \tag{5.20}$$

The control input with linear component and the adaptive augmentation is,

$$u(t) = -Kx + \theta x + K_D \dot{\theta} x \tag{5.21}$$

5.4 Simulation Studies

Simulations have been performed on the HSV by trimming the vehicle at $h = 85\ 000$ ft and Mach 8. The HSV is commanded to track a reference trajectory which results in a step change of 1000 ft in altitude and 100 ft in velocity. At the start of the simulation, the CG is statically shifted by Δx and the HSV is commanded a desired trajectory in velocity and altitude. This experiment is more demanding that a slow time varying shift of the center of gravity. The hypersonic vehicle has a reference chord (mean aerodynamic chord) of 17 ft. The aim of the control design is to accommodate forward and backward CG shits close to 10% of the reference chord. It should be noted that the standard notion that forward CG movements are stabilizing is not true in general for the hypersonic vehicles. This is mainly due to the fact that the pitching moment and the flexible states are coupled. Thus CG movement in backward or forward direction might excite the flexible dynamics and cause the HSV to become unstable.

Figures 5-5 through 5-8 show that this indeed is the case and compares the performance of linear and adaptive controllers for a forward CG shift of $\Delta x = 1$ ft while tracking a commanded trajectory in the $V - h$ space. It was found that without adaptive augmentation, the linear controller was unable to stabilize the HSV even for small CG shifts, $\Delta x = \pm 0.5$ ft. The adaptive controller on the other hand could track the reference trajectory for CG shifts of $-1 < \Delta x < 1.5$ ft. As a negative CG shift (CG moving backwards), makes the closed loop plant with linear feedback unstable, adding non-linear damping to the system was observed to be very helpful.

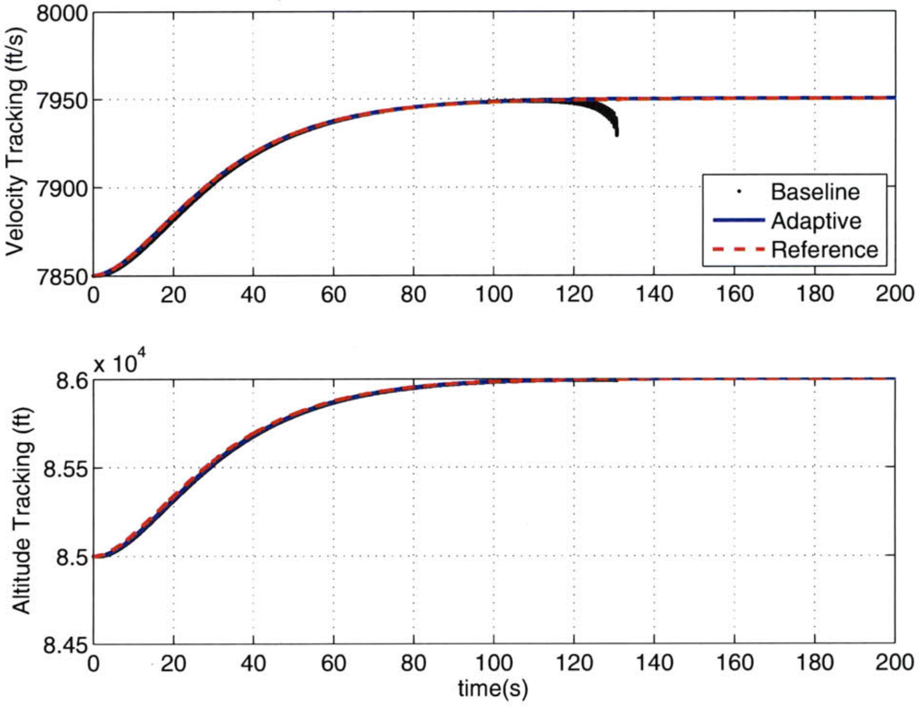

Figure 5-5: Tracked States : Velocity and Altitude

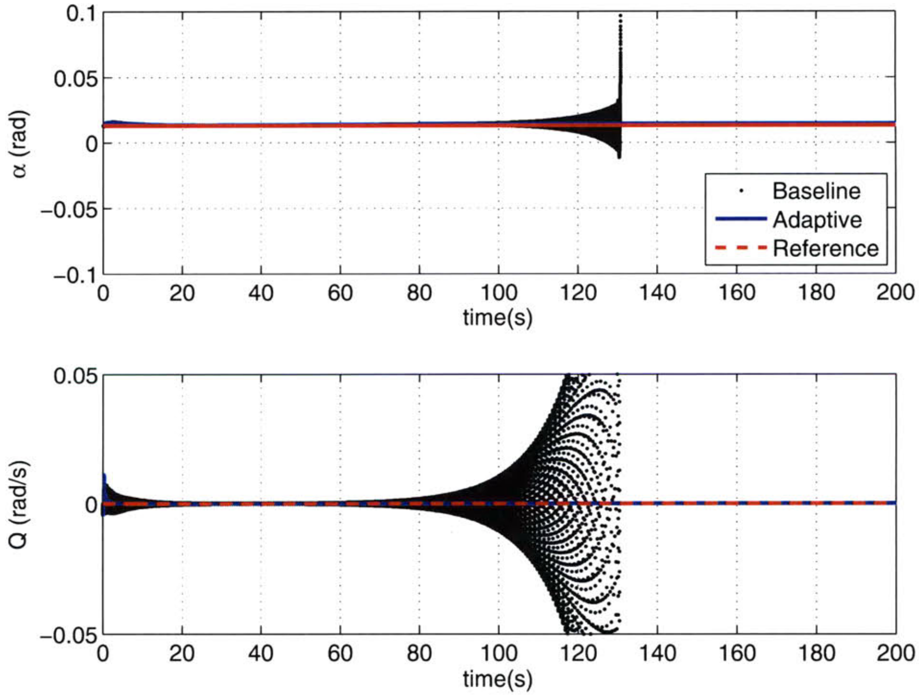

Figure 5-6: Angle of attack and Pitch rate

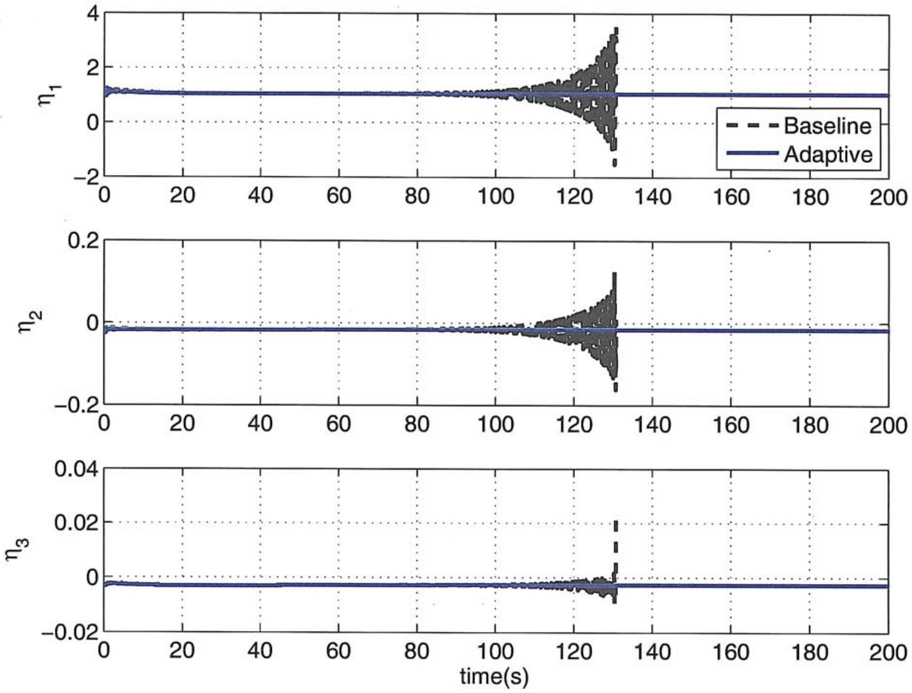

Figure 5-7: Flexible States

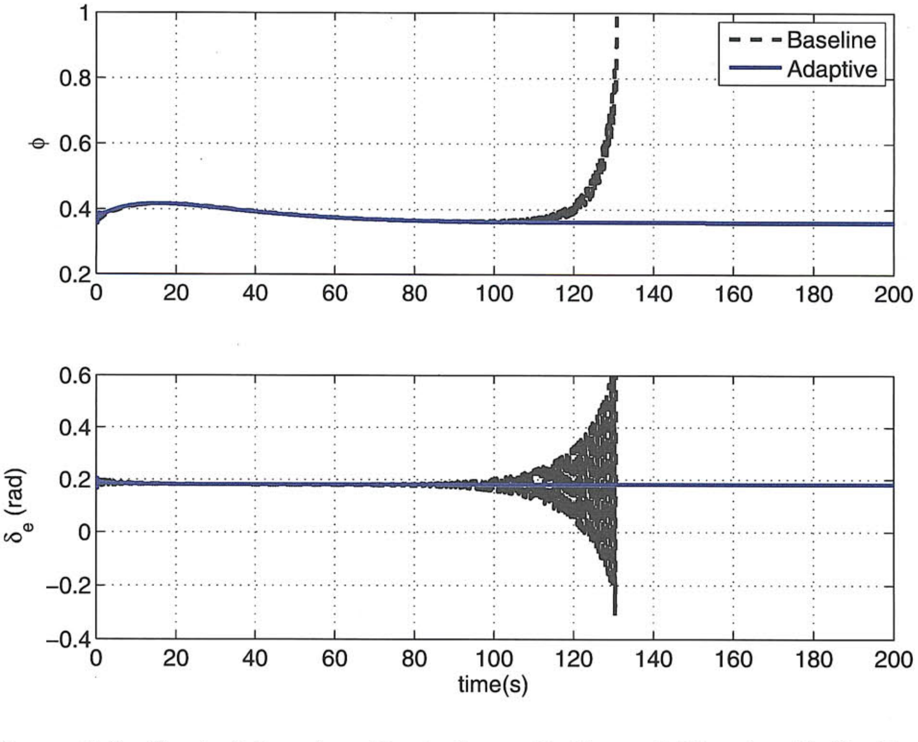

Figure 5-8: Control Inputs : Equivalence Ratio and Elevator Deflection

Chapter 6

Conclusion

The main contributions of this thesis are described below :

(i) **Adaptive controllers for actuation uncertainties** : The thesis develops adaptive controllers which guarantee global stability for linear plants in presence of actuation uncertainties. For linear plants with dynamics,

$$\dot{x} = Ax + Bu$$

actuation uncertainties can be defined as those uncertainties that lead to variations in the control matrix B. It is well known that currently available multivariable adaptive controllers give local stability results for a general unknown B. This work derives globally stable controllers for the cases when uncertainties in B can be represented as (i) $B = B_p\Lambda$ (ii) $B = \Lambda B_p$, where B_p is known and Λ is unknown. The first case models uncertainties that can occur due to actuator failures resulting in loss of actuator effectiveness. The second case can be used to model uncertainties that occur due to anomalies in the plant dynamics.

(ii) **Adaptive control with nonlinear damping** : The control input for conventional adaptive controllers is of the form $u = \theta(t)x$, where $\theta(t)$ is a time varying gain. This work introduces a novel idea of using adaptive parameter rate feedback of the form,

$$u = \theta(t)x + K_D\dot{\theta}(t)x$$

where K_D is a positive definite matrix. As $\theta(t)$ is a nonlinear function of state x and error e, addition of the term leads to nonlinear damping and results in a significant increase in performance.

(iii) **Application to Hypersonic Vehicles** : Using the above tools, this work designs stable controllers for hypersonic vehicles in presence of aerodynamic and center of gravity uncertainties. A model that accurately captures the effect of CG shifts on the longitudinal dynamics of the HSV is derived from first principles. Simulation studies performed on a full scale nonlinear model of the HSV show that CG shifts that can be tolerated by hypersonic vehicle can almost be doubled by using an adaptive controller as compared to a fixed gain controller while tracking reference commands in velocity and altitude.

Appendix A

Hypersonic Vehicle Data

	Co-efficient	Value	Units
Geometry	m	170	slugs ft^{-1}
	l	100	ft
	l_f	47	ft
	l_u	20	ft
	l_a	33	ft
	h_i	3.5	ft
	A_d	2	-
	A_n	6.35	-
	$\tau_{1,u}$	3	deg
	$\tau_{1,l}$	6.2	deg
	τ_2	14.4	deg
	A_e	3.5	ft^2 × ft
	I_{yy}	8.6722×10^{4}	slugs ft^2/rad
	z_T	8.6722	ft
	$\bar{c}$	17	ft
	S	17	ft^2 × ft^{-1}
Atmosphere	h_0	8.5×10^{4}	ft
	ρ_0	6.743×10^{-5}	slugs/ft^{-3}
	h_s	2.136×10^{4}	ft

Table A.1: Geometric and Atmospheric Data

	Co-efficient	Value	Units
Lift	C_L^{α}	5.96×10^{0}	rad^{-1}
	C_L^{0}	-2.4377×10^{-2}	–
	$C_L^{\delta_e}$	9.2176×10^{-1}	rad^{-1}
	$C_L^{\eta_1}$	-3.4102×10^{-2}	ft^{-1}
	$C_L^{\eta_2}$	-3.1737×10^{-2}	ft^{-1}
	$C_L^{\eta_3}$	-6.7580×10^{-2}	ft^{-1}
Drag	$C_D^{\alpha^2}$	7.9641×10^{0}	rad^{-2}
	C_D^{α}	-7.4020×10^{-2}	rad^{-1}
	C_D^{0}	1.988×10^{-2}	–
	$C_D^{\delta_e^2}$	9.1021×10^{-1}	rad^{-2}
	$C_D^{\delta_e}$	1.0840×10^{-6}	rad^{-1}
	$C_D^{\eta_1}$	1.2934×10^{-3}	ft^{-1}
	$C_D^{\eta_2}$	2.5523×10^{-4}	ft^{-1}
	$C_D^{\eta_3}$	2.7066×10^{-3}	ft^{-1}
Moment	$C_M^{\alpha^2}$	6.8888×10^{0}	rad^{-2}
	C_M^{α}	5.139×10^{0}	rad^{-1}
	C_M^{0}	1.627×10^{-1}	–
	$C_M^{\delta_e}$	2.7326×10^{0}	rad^{-1}
	$C_M^{\eta_1}$	-7.1776×10^{-3}	ft^{-1}
	$C_M^{\eta_2}$	-3.0220×10^{-2}	ft^{-1}
	$C_M^{\eta_3}$	-1.0666×10^{-2}	ft^{-1}
Thrust	$C_T^{\phi\alpha^3}$	-1.4038×10^{1}	rad^{-3}
	$C_T^{\phi\alpha^2}$	-1.5839×10^{0}	rad^{-2}
	$C_T^{\phi\alpha}$	6.9341×10^{-1}	rad^{-1}
	C_T^{ϕ}	1.9904×10^{-1}	–
	C_T^{3}	1.0929×10^{0}	rad^{-3}
	C_T^{2}	9.7141×10^{-1}	rad^{-2}
	C_T^{1}	3.7275×10^{-2}	rad^{-1}
	C_T^{0}	-2.1635×10^{-2}	–
	$C_T^{\eta_1}$	-2.7609×10^{-3}	ft^{-1}
	$C_T^{\eta_2}$	-3.4979×10^{-3}	ft^{-1}
	$C_T^{\eta_3}$	-5.3310×10^{-3}	ft^{-1}

Table A.2: Lift, Drag, Thrust and Moment co-efficients

	Co-efficient	Value	Units
Mode 1	$N_1^{\alpha^2}$	-8.9274 × 10 $^{-2}$	lb × ft^{-1} × slug$^{-0.5}$ × rad^{-2}
	N_1^{α}	3.4971 × 10 $^{-1}$	lb × ft^{-1} × slug$^{-0.5}$ × rad^{-1}
	N_1^{0}	2.7562 × 10 $^{-3}$	lb × ft^{-1} × slug$^{-0.5}$
	$N_1^{\delta_e}$	3.9029 × 10 $^{-2}$	lb × ft^{-1} × slug$^{-0.5}$ × rad^{-1}
	$N_1^{\eta_1}$	-9.3415 × 10 $^{-4}$	
	$N_1^{\eta_2}$	-6.7015 × 10 $^{-4}$	
	$N_1^{\eta_3}$	-1.8813 × 10 $^{-3}$	
Mode 2	$N_2^{\alpha^2}$	8.8374 × 10 $^{-2}$	lb × ft^{-1} × slug$^{-0.5}$ × rad^{-2}
	N_2^{α}	9.5685 × 10 $^{-2}$	lb × ft^{-1} × slug$^{-0.5}$ × rad^{-1}
	N_2^{0}	1.3834 × 10 $^{-3}$	lb × ft^{-1} × slug$^{-0.5}$
	$N_2^{\delta_e}$	-2.4875 × 10 $^{-2}$	lb × ft^{-1} × slug$^{-0.5}$ × rad^{-1}
	$N_2^{\eta_1}$	4.112 × 10 $^{-4}$	
	$N_2^{\eta_2}$	1.0924 × 10 $^{-4}$	
	$N_2^{\eta_3}$	8.5621 × 10 $^{-4}$	
Mode 3	$N_3^{\alpha^2}$	-7.4826 × 10 $^{-2}$	lb × ft^{-1} × slug$^{-0.5}$ × rad^{-2}
	N_3^{α}	1.0299 × 10 $^{-1}$	lb × ft^{-1} × slug$^{-0.5}$ × rad^{-1}
	N_3^{0}	-1.9277 × 10 $^{-3}$	lb × ft^{-1} × slug$^{-0.5}$
	$N_3^{\delta_e}$	-4.2624 × 10 $^{-3}$	lb × ft^{-1} × slug$^{-0.5}$ × rad^{-1}
	$N_3^{\eta_1}$	3.2963 × 10 $^{-4}$	
	$N_3^{\eta_2}$	3.022 × 10 $^{-4}$	
	$N_3^{\eta_3}$	6.5423 × 10 $^{-4}$	

Table A.3: Elastic co-efficients

Bibliography

[1] www.dfrc.nasa.gov/gallery/graphics/x-43a/index.html. *NASA Dryden Flight Research Center Graphic Files.*

[2] Barris Fidany, Maj Mirmirani, and Petros A. Ioannoux. Flight dynamics and control of air-breathing hypersonic vehicles: Review and new direction. In *AIAA International Conference on Space Planes and Hypersonic Systems and Technologies*, 15 - 19 December 2003, Norfolk, Virginia.

[3] Paul L. Moses, Vincent L. Rausch, Luat T. Nguyen, and Jeryl R. Hill. Nasa hypersonic fight demonstrators - overview, status, and future plans. In *Acta Astronautica*, volume 55, pages 619– 630, 2004.

[4] Kumpati S. Narendra and Anuradha M. Annaswamy. *Stable Adaptive Systems.* Dover Publication, Inc., Mineola New, York, 1989.

[5] L. Fiorentin, A. Serrani, M. A. Bolender, and D. B. Doman. Nonlinear robust adaptive control of flexible air-breathing hypersonic vehicles. *Journal of Guidance, Control, and Dynamics*, 32(2), 2009.

[6] M. Kuipers, P. Ioannou, B.Fidan, and M. Mirmirani. Robust adaptive multiple model controller design for an airbreathing hypersonic vehicle model. In *AIAA Guidance, Navigation, and Control Conference and Exhibit*, 18-21 August 2008. Honolulu,Hawaii.

[7] D. Sigthorson, A. Serrani, S. Yurkovich, M. Bolender, and D. Doman. Tracking control for an overactuated hypersonic air-breathing vehicle with steady state constraints. In *AIAA Guidance Navigation and Controls Conference and Exhibit*, Aug. 21-24 2006. Keystone, Colorado.

[8] Travis E. Gibson and Anuradha M. Annaswamy. Adaptive control of hypersonic vehicles in the presence of thrust and actuator uncertainties. In *AIAA Guidance, Navigation, and Control Conference and Exhibit*, 18-21 August 2008. Honolulu,Hawaii.

[9] Qian Wang and Robert F. Stengel. Robust nonlinear control of a hypersonic aircraft. *Journal of Guidance, Control, and Dynamics*, 23(4), Jul-Aug 2000.

[10] Qian Wang and Robert F. Stengel. Robust control of nonlinear systems with parametric uncertainty. *Automatica*, 38:1591–1599, 2002.

[11] Travis E. Gibson and Anuradha M. Annaswamy. Adaptive control of hypersonic vehicles in the presence of thrust and actuator uncertainties. In *AIAA Guidance, Navigation, and Control Conference and Exhibit*, 18-21 August 2008. Honolulu,Hawaii.

[12] Barton J. Bacon and Irene M. Gregory. General equations of motion for a damaged asymmetric aircraft. *AIAA Atmospheric Flight Mechanics Conference and Exhibit*, 20-23 Aug 2007. Hilton Head, South Carolina.

[13] J. Jang, A. M. Annaswamy, and E. Lavretsky. Adaptive flight control in the presence of multiple actuator anomalies. In *Proceedings of the 2007 American Control Conference*, pages 3300–3305, New York, NY,20-23 August 2007.

[14] J. Jang, A. M. Annaswamy, and E. Lavretsky. Adaptive control of time-varying systems with gain-scheduling. In *Proceedings of the 2008 American Control Conference*, Seattle, WA, June 2008.

[15] Michael A. Bolender and Davod B. Doman. Flight path angle dynamics of air-breathing hypersonic vehicles. In *AIAA Guidance, Navigation, and Control Conference and Exhibit*, 21-24 August 2006. Keystone,Colorado.

[16] J.T. Parker, A. Serrani, S. Yurkovich, M. Bolender, and D. Doman. Control-oriented modeling of an air-breathing hypersonic vehicle. *Journal of Guidance, Control, and Dynamics*, 30(3), May-June 2007.

[17] Michael A. Bolender and David B. Doman. Nonlinear longitudinal dynamical model of an air-breathing hypersonic vehicle. *Journal Spacecraft and Rockets*, 44(2), March-April 2007.

[18] Michael A. Bolender, Michael W. Oppenheimer, and David B. Doman. Flight path angle dynamics of air-breathing hypersonic vehicles. In *AIAA-2006-6692, Aug. 21-24, 2006.*

[19] M. Oppenheimer, T. Skujins, M. Bolender, and D. Doman. A flexible hypersonic vehicle model developed with piston theory. In *AIAA Atmospheric Flight Mechanics Conference and Exhibit.* AIAA-2007-6396, Aug. 20-23 2007. Hilton Head, South Carolina.

[20] T. Williams A. Culler and M. Bolender. An aerothermal flexible mode analysis of a hypersonic vehicle. In *AIAA GNC -2007-6395.*

[21] Michael A. Bolender and David B. Doman. Effects of unsteady and viscous aerodynamics on the dynamics of a flexible air-breathing hypersonic vehicle. In *AIAA GAFMC*, August 2007. Hilton Head, South Carolina.

[22] M. Oppenheimer, D. Doman, J. McNamara, and A. Culler. Viscous effects for a hypersonic vehicle model. In *AIAA-2008-6382*, Aug. 18-21, 2008.

[23] L. Fiorentini, A. Serrani, Michael A. Bolender, and David B. Doman. Nonlinear robust/adaptive controller design for an air-breathing hypersonic vehicle model. In *AIAA Atmospheric Flight Mechanics Conference and Exhibit*, Aug. 20-23 2007. Hilton Head, South Carolina.

[24] L. Fiorentini, A. Serrani, Michael A. Bolender, and David B. Doman. Nonlinear control of a hypersonic vehicle with structural flexibility. In *IEEE Conference on Decision and Control*, 2008.

[25] Karl D. Bilimoria and David K. Schmidt. Integrated development of the equations of motion for elastic hypersonic flight vehicles. *Journal of Guidance, Control, and Dynamics*, , 0731-5090 vol.18 no.1 (73-81), 1995.

[26] Newman Brett and David K Schmidt. Aeroelastic vehicle multivariable control synthesis with analytical robustness evaluation. *Journal of Guidance, Control, and Dynamics*, 0731-5090 vol.17 no.6 (1145-1153), 1994.

[27] Frank R. Chavez and David K. Schmidt. Analytical aeropropulsive/aeroelastic hypresonic-vehicle model with dynamic analysis. *Journal of Guidance, Control, and Dynamics*, 17(6), Nov-Dec 1994.

[28] S. Torrez, N. Scholten, M. Bolender J. Driscoll, M. Oppenheimer, and D. Doman. Dynamics of hypersonic vehicles: Shift of poles / zeros by improved propulsion modeling. In *AIAA-2008-6386*, Aug. 18-21 2008.

[29] S. Torrez, N. Scholten, D. Micka, J. Driscoll, M. Bolender D. Doman, and M. Oppenheimer. A scramjet engine model including effects of precombustion shocks and dissociation. In *AIAA-2008-4619*, July 21-23 2008.

[30] John D. Anderson. *Modern Compressible Flow: with Hystorical Perspective.* McGraw-Hill Science, 2002.

[31] H. Ikawa. Rapid methodology for design and performance prediction of integrated supersonic combustion ramjet engine. 17(3):437, 1991.

[32] Anon. *Handbook of Aviation Fuel Properties.* Coordinating Research Council, Atlanta, GA, 1983.

[33] Leonard Meirovitch. *Fundamentals of Vibrations.* Mc Graw Hill, 2001.

[34] J. Jang, A. M. Annaswamy, and E. Lavretsky. Adaptive control of time-varying systems with gain-scheduling. In *Proceedings of the 2008 American Control Conference*, Seattle, WA, June 2008.